Final Report of Research Project

of

National Science Council

Temporal and spatial variations of Kuroshio off southeast and southwest of Taiwan

89-2611-M-002-031-OP2

黑潮於台灣東南、西南海域的時空變化

By
T. Y. Tang
唐存勇

國立台灣大學

Institute of Oceanography
National Taiwan University
Taipei, Taiwan, ROC

Research Project No: NSC 89-2611-M-002-031-OP2

May 2002

1. Introduction:

Around 15°N, the westward North Equatorial Current (NEC) in Pacific Ocean was blocked by the continent of Philippines, and divided into two branches. One, named as Mindanao Current, flowed southward. The other one, named as Kuroshio, flowed northward along the eastern coast of Luzon. As Kuroshio leave the northern tip of Luzon, it encountered its first meridional gap, Luzon Strait. Whether the Kuroshio intruding into the SCS or leaping across the Luzon Strait is quite controversial. Wyrtki (1961) and Nitani (1972) indicated that the KC intruded into the SCS when the northeast monsoon was prevailed and such intrusion was halted as the southwest monsoon was in vogue. This seasonal intrusion feature was re-confirmed by many pioneers. For example, Shaw (1991) analyzed historical hydrographic measurements, and Farris and Wimbush (1996) examined the satellite-derived Sea Surface Temperature (SST) images reached the similar result; the KC intrusion occurred seasonally. However, Qu (2000) estimated the seasonal volume transport of Kuroshio intrusion using the historical temperature profile. His estimates varied seasonally, but always westward. The intruded volume was 5.5 Sv in summer and 0.9Sv in winter. Similar result was also found in the numerical model result of Metzger et al (1996). Although they did not claim explicitly, their results implicitly indicated the KC could intrude into the SCS all year round.

The mechanisms caused the KC intrusion were also controversial. Stommel and Aron (1960) claimed that the western boundary current always intruded as it encountered a meridional gap since the β advection. Sheremet (2001) indicated that the KC could leap across the meridional gap as the gap is small or the inertia is large. Analyzed the hydrographic measurements, Wang and Chern (1987) postulated the Ekman transport, induced by the monsoon, could be important for the KC intrusion. The current in the SCS also could be a factor caused or halted the KC

intrusion (Shaw and Chao, 1994). Qu (2000) and Metzger and Hurlburt (1996) concluded that the Kuroshio intrusion was mainly related with the meridional pressure gradient across the LS. All of the controversies are largely cause by the insufficient data, especially the long-term moored current velocity measurement.

Owing to the behavior of Kuroshio in the region of Luzon Strait is critical to the understanding of current around Taiwan; the controversy needs to be clarified. In attempt to do so, we promised to explore the current south of Taiwan. 5 moorings had been deployed and 2 large-scale hydrographic surveys had been taken. The preliminary is reported here.

2. Fieldwork:

Three ADCP and one Atlas moorings had been deployed west of Luzon Strait. The ATLAS mooring was lost due to the unknown reason. It is the first lose since the PI deployed the ATLAS mooring on 1997. The one, named as L4, deployed prior the project was funded. The data length, collected from L4, was around 9 months, from May 2000 to Feb. 2001. The other two moorings, named as L5 and L6, deployed at southern opening of Taiwan. Their data length was over 6 months, from Oct. 2000 to Apr. 2001. One ADCP mooring was deployed east of Taiwan joining with Prof. Joe Wang's mooring array. This mooring were deployed and retrieved successfully, but the pressure sensor was out of work. The current velocity recorded by the ADCP had to read using a special way, which was developed by Donvanan and Weisberg (2002, personal communication). The data is not available to be presented here.

In additional to mooring deployment, 2 large hydrographic surveys had been done. The snapshot current velocities along two zonal and one meridional transits were recorded by Ship-board ADCP. Meanwhile, the CTD measurements along the

transits were performed. The interval of CTD stations varied. The cast was down to 1500m. The absolute geostrophic current velocity was calculated by using the CTD and Sb-ADCP measurements. The result was used to compare to the TOPEX altimetry. The first survey was quite successful, but he second one had deficiency. The typhoon halted the survey near northern Luzon.

3. Spatial structure of Kuroshio:

Two ways were used to study the spatial structure of Kuroshio around Taiwan. The first way is to collect and edit the current velocity recorded by Sb-ADCP. This work is cooperated with the Ocean Data Bank (ODB) of National Center for Ocean Research (NCOR). The ODB provided the Sb-ADCP data obtained form OR1, 2, and 3. We edited, debug, and analyzed the data. We also provided ODB with the data process software for their future usage. A composite current velocity distribution around Taiwan was obtained. It provided a chance to examine the spatial characters of Kuroshio around Taiwan. The composite current velocity was validated by compared with the moored current velocity. A manuscript has been submitted to Journal (Deep Sea Research) for publication. Positive comments were obtained. Both reviewers recommended for publication with minor revision. The manuscript is attached as Appendix. The details of work and findings were stated in there. The result of this part of research is not stated here.

Since the composite Sb-ADCP current velocities were confined in the upper (<350m) ocean, the Kuroshio below upper-ocean remains unclear. The second way to study the spatial structure of Kuroshio used the CTD and snapshot Sb- ADCP measurements. Using the hydrographic data to study the Kuroshio is a popular and old way. It usually obtained the relative velocity instead of absolute velocity since the velocity at reference was unknown. The Sb-ADCP velocity in 50-100m was

used as a reference velocity in this study. The absolute velocity was obtained. Figure 3-1 shows the north component velocities along 18°N. The velocities obtained from Sb-ADCP (upper panel) and estimated geostrophic velocity (lower panel). The upper panel shows the velocity in the upper 300m. The low panel shows the velocity from the surface to 1500m. The two velocity distributions are alike, but the former one had fine spatial structure. The geostrophic velocity acted a low-wavenumber-pass filtered velocity. The Kuroshio flowed close to the continent (northern Luzon). It had maximum speed over 100cm/s. Its width and influence depth were 100km and 300m, respectively. Below the 300m, a southward countercurrent was seen. This result indicates that upstream Kuroshio had large speed, but it was narrow and shallow. Similar to Figure 3-1, Figure 3-2 shows the velocities along 23.5°N. East of Taiwan, the Kuroshio south of I-Lan Ridge had relative slow speed, but it became wider and deeper. The maximum speed obtained from SB-ADCP was over 100cm/s, but the low-wavenumber-pass filtered geostrophic speed was less than 80cm/s. The northward transport of Kuroshio increased since it left northern Luzon. The increase of volume transport mainly originated from the east. Figure 3-3 shows the Sb-ADCP current velocity at 16m along the cruise track. The current along 127°E mainly was westward. It could be a source of the increase of volume transport of Kuroshio when it flowed to the north. The anomalies of TOPEX/ERS-2 altimetry are also shown. Some agreement was found between the altimetry anomaly and Sb-ADCP current velocity. For example, a negative anomaly located at southwest corner of cruise track, where cyclonic flow was displayed. However, some contradictions were also found. Moreover, the anomaly calculated by two well-know organizations was against each other's. This result indicates that the altimetry anomaly should be careful to be used. The second survey had similar result with the first one. Its results are not presented. Dr. Y. J. Yang and I are using

these data writing a manuscript.

4. Moored observation

Figure 4-1 shows the hourly U and V at 50m and 150m on L4, where is 300km west of center LS. The length of recorded velocity time series was around 9 months, May 2000 – Jan. 2001. Although the length was shorter than one year, it covered the seasons of SW and NE monsoon. The hourly U and V were dominated by the high frequency fluctuations. The low-frequency variation was hard discernable. The spectra analysis showed the high-frequency fluctuations were mainly inertia, diurnal, and semi-diurnal tidal currents. They were primarily barotropic. No distinguishable peak was clearly seen in the sub-inertia frequency band. Using the low-pass filter, the high frequency (period shorter than 48 hrs) fluctuations were removed from the hourly U and V time series. The low-frequency variation was then examined.

Figure 4-2 shows the 48-hour low-pass filtered U and V. The velocity contours are function of depth and time. The westward current dominated in U. The eastward current was seen, but it only appeared in short period. The most notable eastward current was in August, when the westward propagating was favorably presented in the northern SCS (Metzger and Hurlburt, 2002). Again, no clearly seasonal difference was found. The V was generally weak. It changed its sign around every 10-45 days, but the time scale varied. Similar to U, the V had no clearly seasonal difference. However, the V seems had large fluctuation during the season of NE monsoon. The depth (30-170m) averaged U was fluctuated but was westward in the most of time. The largest speed was over 60cm/s. The eastward velocity was found in August. It was seen occasionally in the rest of months. The depth averaged V was also fluctuated. Its negative and positive values appeared

nearly even. Nonetheless, the northward velocity seems to be favored in the season of NE monsoon. The spectra of U and V had no discernible peak at specific frequency. The current velocity fluctuated at various time scales. The velocity sticks show that the directions of current varied from the 2 nd to 3 rd quadrant mostly. This result indicates that the current at L4 primarily flowed into the SCS.

The hourly U and V at L5 and L6 are shown in Figure 4-3a and b, respectively. The recorded length was around 6 months, Oct. 2000 – Apr. 2001. The spectra analysis indicates that the semi-diurnal and diurnal tidal current dominated the high-frequency fluctuations. The two tidal current had similar amplitude at L5, while the semi-diurnal tidal current had larger amplitude than diurnal tidal current at L6. The inertia motion was not clearly separated from the diurnal tidal motion. Again, the tidal current was primarily barotropic. No distinguishable variance peak was seen in the sub-tidal frequency band.

Figure 4-4 shows the 48-hour low-pass filtered U and V. The velocity contours are function of depth and time. Except two eastward velocity surges, the U at L5 was generally weak and favored to be westward. The two eastward surges were In Dec. and March. Their durations were around one month. The maximum speeds of these eastward velocity surges were around 100cm/s. The V also had two northward velocity surges. These two surges leaded the surges of U around 10-15 days. Except these two surges, the V was negative/positive alternatively. Because the measurements were made principally in the season of NE monsoon, the seasonal variation is unknown. The depth (30-130m) averaged U and V fluctuated at various time scales. No significant peak found in their variance spectra. The velocity sticks show that the positive (negative) U frequently occurred with positive (negative) V. The northwestward or southeastward current was not seen commonly. The positive/negative of U at L6 was shown reciprocally, but the positive U had longer

duration and larger amplitude than the negative U. The largest U was generally at uppermost depth and decreased with the depth. Similarly, the positive/negative of V at L6 appeared reciprocally, but the negative V had longer duration and larger amplitude than the positive V. The velocity decreased with depth. The depth (20-180m) averaged velocity showed that the positive (negative) U occurred nearly consistently with the negative (positive) V. The current was either directed to southeastward or northwestward, in generally. It is noted that the positive (negative) V at L6 occurred in favor with negative (positive) V at L5. This result suggested that the clockwise current at the southern opening of Taiwan Strait, which shown in the composite Sb-ADCP current velocity distribution, could be reversed once in a while.

5. Numerical model

A numerical model, Miami Isopycnic Coordinate Ocean Model (MICOM), with large domain was adapted to study the Kuroshio around Taiwan. Dr. Wen-Der Liang, a former PHD student of Dr. W.-S. Chuang and I, spent 2 years to establish the model in the Institute of Oceanography, National Taiwan University. In the progress of model establishment, we learned that the model domain has to be large enough to generate the true western boundary current, such as Kuroshio. The model domain is from 95°E to 160°E and from 20.8°S to 45.1°N. The grid size is 0.25°x0.25°. The initial condition obtained from the World Ocean Atlas 1994 (Levitus and Boyer, 1994). No-slip boundary condition was applied. The details of model were stated in Liang's dissertation (2002). The model was forced by climatologically model wind, obtained from European Center for Medium-range Weather Forecast (ECMWF), for 10 year. After the model was spin-up, a monthly ECMWF wind was applied to assist the interpretation of moored observation. The dissertation of Liang (2002) showed the details of model.

A number of moored observations were applied to confirm the validation of numerical model output. The observations included 3 moored current velocities in the Luzon Strait, named L1, 2, and 3, and 3 moored current velocities west of Luzon Strait, L4, 5, and 6. Figure 5-1 shows the comparison between model output and observed depth-averaged velocities comparison at L1, 2, and 3. 5-day convolution average was applied. At L1 and L2, the model results represented properly the mean and annual evolution of observed current velocity. The difference of mean velocities was small. Only slight difference found in U at L1 and V at L2. The annual variation was small in both model and observed velocities. However, without the model output assist, such small annual variation was intricately discernible. The high-frequency fluctuations, several days to a couple month time scales, were not found in the model output. This could be mainly related with that the monthly wind was used to force the model. The agreement between the model and observed velocities at L3 was not as good as it at L1 and L3. In despite of the high frequency fluctuations, the model V at L3 was similar with the observed V, but not for U. The mean of observed U was nearly zero, while the mean of model U was –30cm/s. Although the westward velocity at L3 was smaller than it at L2, it showed that the Kuroshio still intruded into the SCS through L3. This result is different from the observation, which indicated L3 was a southern boundary of Kuroshio intrusion. The southern boundary in the model result was south of L3. The difference could be related with the coarse model resolution. The islands in southern Luzon Strait were not represented properly. Nonetheless, the evolutions of current velocity at L3 in model and observation were still alike.

Figure 5-2 show the model-observation comparison at L4, 5, and 6 (west of Luzon Strait). The agreement was not as good as the comparison in Luzon Strait. The observation was dominated by the intra-seasonal fluctuations, which the model

was incapable to represent. However, the means and annual evolutions of model output were similar to them of observations. For example, the westward component velocity was a nearly persistent feature in both the model output and observation at L4. The clockwise flow pattern, which was dimly seen in the observation, was clearly represented in the model output. The model-observation comparison in the central South China Sea (not shown) was also examined. The model output properly represented the annual and inter-annual evolutions of observed thermal and velocity. Therefore, we concluded that the model output was validated to use for the study of annual and inter-annual variations of Kuroshio south of Taiwan.

6. Kuroshio Intrusion

The current velocity distributions obtained from model outputs in the region of 105-130°E, 0-30°N at June and December on Year 10 are shown in Figure 6-1. Six solid dots indicate the locations of observed current velocities. In June, the westward North Equatorial Current (NEC) in western Pacific was mainly in the region of 10-15°N. It disunited into the northward Kuroshio and southward Mindanao Current around 13°N as it approached to Mindanao. The Kuroshio flowed essentially along the eastern coast of Philippine to the north. The westward NEC continuously poured into the Kuroshio until 17°N, where the strength (speed over 70cm/s) of Kuroshio was gained. The northward Kuroshio bent, but not immediately to northwestward as it leaves Luzon. The inertia effect might keep the swift Kuroshio flowed along with its original direction when it immediately dropped out its western continental boundary. Meanwhile, the Kuroshio also could be prevented from immediately curved by an eastward current west of southern LS. This eastward current was a part of cyclonic flow in the northern SCS. This cyclonic flow varied seasonally and had great influence on the intruded Kuroshio. To

distinguish this cyclonic flow with other small cyclonic flows, it is referred as SCS cyclonic flow, hereafter. After intrusion, the Kuroshio separated into two branches. One branch curved clockwisely and then flowed along the eastern coast of Taiwan to the north. The other branch interacted with the cyclonic flow south of southern opening of Taiwan Strait, and then gradually merged with the SCS cyclonic flow and became a part of this flow in the northern SCS. The intruded Kuroshio was re-cycled with the SCS cyclonic flow. No significant Kuroshio entered either Taiwan Strait or further inside of SCS. The current in Taiwan Strait was originated from the northern shelf break or even could be traced down to the western boundary of Vietnam.

The main feature of Kuroshio intrusion in December was similar, but had notable differences, from it in June. In December, the zonal region of NEC expanded northward largely and the origination of Kuroshio moved slight northward. The seasonal expansion/contraction of NEC zonal width in the western Pacific was also seen in the surface current velocity distributions, which obtained from drifting buoys. The westward NEC continuously poured into the Kuroshio from its origination to the northern tip of Luzon. Obviously, more NEC discharged into the Kuroshio. Therefore, the Kuroshio had larger speed and width in December than in June. Unlike in June, the Kuroshio immediately curved to the northwest in December as it dropped out the western continental boundary. The westward NEC pressed on the Kurohsio intrusion could be a reason for the instant bend. The intruded Kuroshio had larger volume and incident angle in December than in June. The SCS cyclonic flow, which was confined in northern SCS on June, was expanded basin-widely on December. It could be treated as two cyclonic flows, one was confined in the southern basin, and one nearly occupied the entire basin. The southern one is temporally ignored in this paper since it had no directly influence on the Kuroshio

intrusion. The SCS cyclonic flow in December presented a northward current west of Luzon as well as southern LS. The intruded Kuroshio interacted firstly with the northward current west of central LS, and then gradually turned cyclonically, finally united with the cyclonic flow entered deeply into the SCS. A small portion of intruded Kuroshio curved clockwisely flowed along the southern opening of Taiwan Strait. It either entered into the Taiwan Strait or flowed out through the southern tip of Taiwan added into the Kuroshio. Contrast to June, the Kuroshio became an important source for the current in Taiwan Strait in December.

To focus on the Kuroshio intrusion, Figure 6-2 shows the current velocity distributions at 50m around Luzon Strait. The figure contains 12 panels (4 rows x 3 columns). In each column, the 4 panels from top to bottom represent the current velocity at 15th of March, June, September, and October. From left to right, the columns represent the current velocity at Year 1997, 1998, and 1999. Again, 6 dots point out the locations of observed current velocities. Firstly, the current velocity distributions in leftmost (Year 1997) are used to illustrate the annual evolution. Then, the inter-annual variation is illustrated by the comparison of current velocity between the columns.

The upper-leftmost panel indicates that the Kuroshio largely intruded into the SCS in March. The northeastward current, which was a part of basin-wide SCS cyclonic flow, west of southern LS was also large. It might push the intruded Kuroshio to the north so that the Kuroshio reached the southern opening of Taiwan Strait. The intruded Kuroshio then curved westward flowing along shelf break into the SCS, finally combined with the SCS cyclonic flow. In June, the SCS cyclonic flow was shrink, confined in the northern SCS. The strength of Kuroshio was reduced and the NEC contracted southward. The Kuroshio intruded into the SCS more westward. After the intrusion, the Kuroshio separated into two branches.

The large one united with the cyclonic flow directed to the west. The other one turned clockwisely partially flowed along the southern opening of Taiwan Strait. This flow partially entered into the Taiwan Strait and partially poured into the Kuroshio through the southern tip of Taiwan. The former was one of sources for the current in Taiwan Strait. The contribution for the current in Taiwan Strait from the northwestward current along the northern shelf was significant. In September, the SCS cyclonic flow moved to the further southwest. The intruded Kuroshio had similar angle in LS as it in June, but it curved rapidly to the west after intrusion. A high-pressure center located immediately south of Taiwan Strait opening could be a reason causing the intruded Kuroshio curved westward. As the SCS cyclonic flow moved westward, a part of current in its northeast corner retroflexed and curved clockwisely to form an anti-cyclonic flow south of Taiwan Strait opening. The intruded Kuroshio merged with the SCS cyclonic flow to further enhance this anti-cyclonic flow. Meanwhile, the anti-cyclonic flow carried the intruded water partially re-added into the Kuroshio and partially entered into the Taiwan Strait. On the south of main intruding pathway, a portion of intruded Kuroshio curved cyclonically, but most of them was retroflexed westwardly feeding into the SCS cyclonic flow. In December, the strength of Kuroshio increased and the zonal region of NEC expanded northward. The Kuroshio intruded deeply into the South China Sea. Meanwhile, a branch of intruded Kuroshio bent northeastwardly flowed into the Taiwan Strait. The Kuroshio could be an important source of Taiwan Strait in winter.

The Kuroshio intrusion in Luzon Strait also had significantly inter-annual variation. The feature mentioned above was in 1997, which was the year of El Nino. In 1998, the year of La Nina, the Kuroshio intrusion was largely reduced. The upper (east of northern Luzon) and down (east of southern Taiwan) streams of Kuroshio

were also reduced. The ocean circulation southwest of Taiwan had different feature than it in El Nino Year. For example, the intruded Kuroshio reached the southern opening of Taiwan Strait and formed a cyclonic circulation south of Taiwan Strait in El Nino Year. It cannot reach the southern opening of Taiwan Strait in La Nina Year. A anti-cyclonic circulation presented south of Taiwan Strait. However, the circulation in the South China Sea (not shown) did not have significant change, but it was slightly weaker. In 1999, the Kuroshio intrusion and it's upper and down streams increased, but did not reach the strength on 1997. The circulation southwest of Taiwan also had different feature than it on 1997 or 1998. The result indicates that the inter-annual variation of Kuroshio could be large. It could have significant impact on the intrusion of Kuroshio in Luzon Strait as well as the down stream of Kuroshio east of Taiwan.

Figure 6-3 shows a few time series obtained from model output. From top to bottom, the panels show the zonal volume transport along 120.75°E, the meridional volume transport along 18.5°N, the zonal transport along 125°E, stick diagram model wind stress and NE-SW component of wind stress time series at L2, and the zonal Ekman volume transport along 120.75°N, respectively. The time series uppermost panel shows the volume transport across the Luzon Strait varied annually and inter-annually. The volume transport of Kuroshio intrusion had distinguished seasonal variation; it was large and small in winter and summer, respectively. The inter-annual variation was also clearly seen. The Kuroshio intruded largely into SCS on the year of El Nino. Such intrusion reduced significantly on the year of La Nina. Since then, the intrusion increased gradually year by year. The amount of Kuroshio intrusion on 2001 was close to it on 1997. It seems that the year of 2002 could be the year of El Nino. Seemingly, the variation of Kuroshio intrusion leads the occurrence of El Nino. During the years of low Kuroshio intrusion, the Kuroshio

mainly leaped across the Luzon Strait. The amount of intruded Kuroshio was less than the amount of SCS outflow in summer. However, the long-term average Kuroshio intrusion in summer was nearly zero.

The meridional volume transport along 18.5°N (second panel) shows the volume transport of upstream of Kuroshio. Though the seasonal variation was seen, it was small in comparison with the inter-annual variation. Such feature is different from the zonal transport across the Luzon Strait. This finding implicitly indicates that the variation of upstream Kuroshio could not be the main factor for the variation of Kuroshio intrusion in Luzon Strait. Move further to the upstream, zonal transport of NEC be shown in third panel. The variation of volume transport of NEC also had large inter-annual variation. The annual variation was seen, but small. The NEC or upstream of Kuroshio had large and small volume transport on El Nina and La Nina years, respectively.

The bottom two panels show the model wind stress at L2 and the Ekman volume transport, which caused by local wind stress. Neither wind stress nor Ekman volume transport had clearly inter-annual variation. The annual variation was dominated. The estimate Ekman volume transport has good correlation with volume transport of intruded Kuroshio, but its amplitude was much smaller than the Kuroshio intrusion. Obviously, the local wind stress could not be a main factor for the Kuroshio intrusion. This conclusion had been reached by Qu (2001). His estimate obtained from the historical hydrographic data.

Figure 6-4 shows the sea surface height A and B, their heights difference. The locations of point are also shown. Point A locates southern Taiwan Strait, while Point B locate northwestern tip of Luzon. The height difference represents the meridional pressure gradient across the Luzon Strait. Both annual and inter-annual variations were found. The zonal geostrophic volume transport estimated from the

pressure gradient had goof correlation as well as similar amplitude with the volume transport of Kuroshio intrusion. This result allows us to make a conclusion that the meriodional pressure gradient could be a main factor for the Kuroshio intrusion. It is worth to note that the variation of pressure gradient mainly originated from the pressure variation at Point B. Such variation was highly correlated with the upwelling west of northern Luzon. A further work is required to explore this feature.

So, far, the validation of numerical model was confirmed. The mechanisms of Kuroshio intrusion seems to be related with the meridional expansion/contraction of NEC and development of upwelling west of northern Luzon. However, a systematic analysis of model result is required making the conclusion solid.

7. Summary:

Thanks for many years support for the field measurement from the National Science Council. The obtained data are able to confirm the model's validation. In the next few years, I plan to concentrate on the dynamic study using the model outputs. The fieldwork would be un-necessary until the observed features are properly interpreted.

Meridional Current along 18°N During October 11~16, 1999

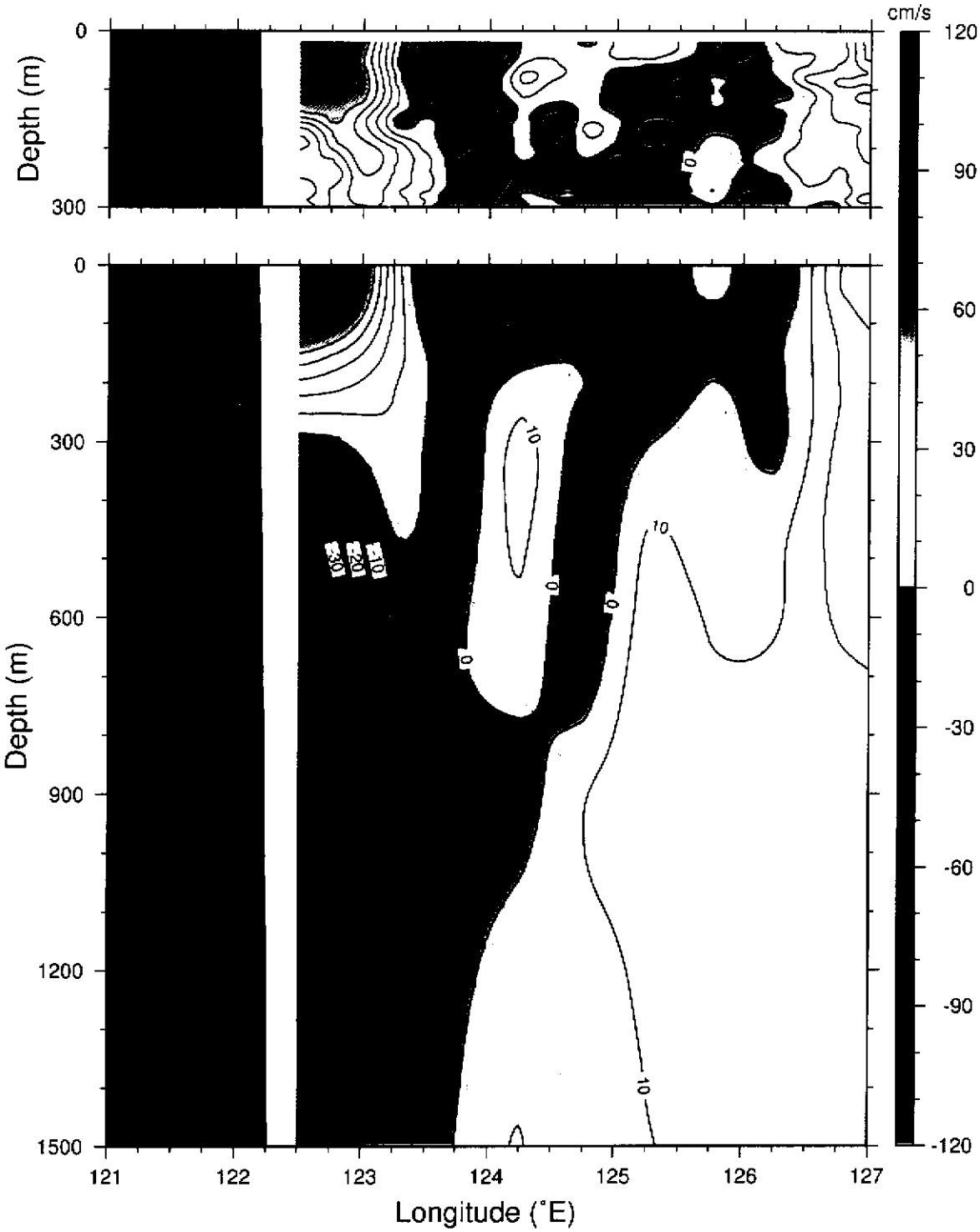

Fig. 3-1

Meridional Current along 23.5°N During October 11~16, 1999

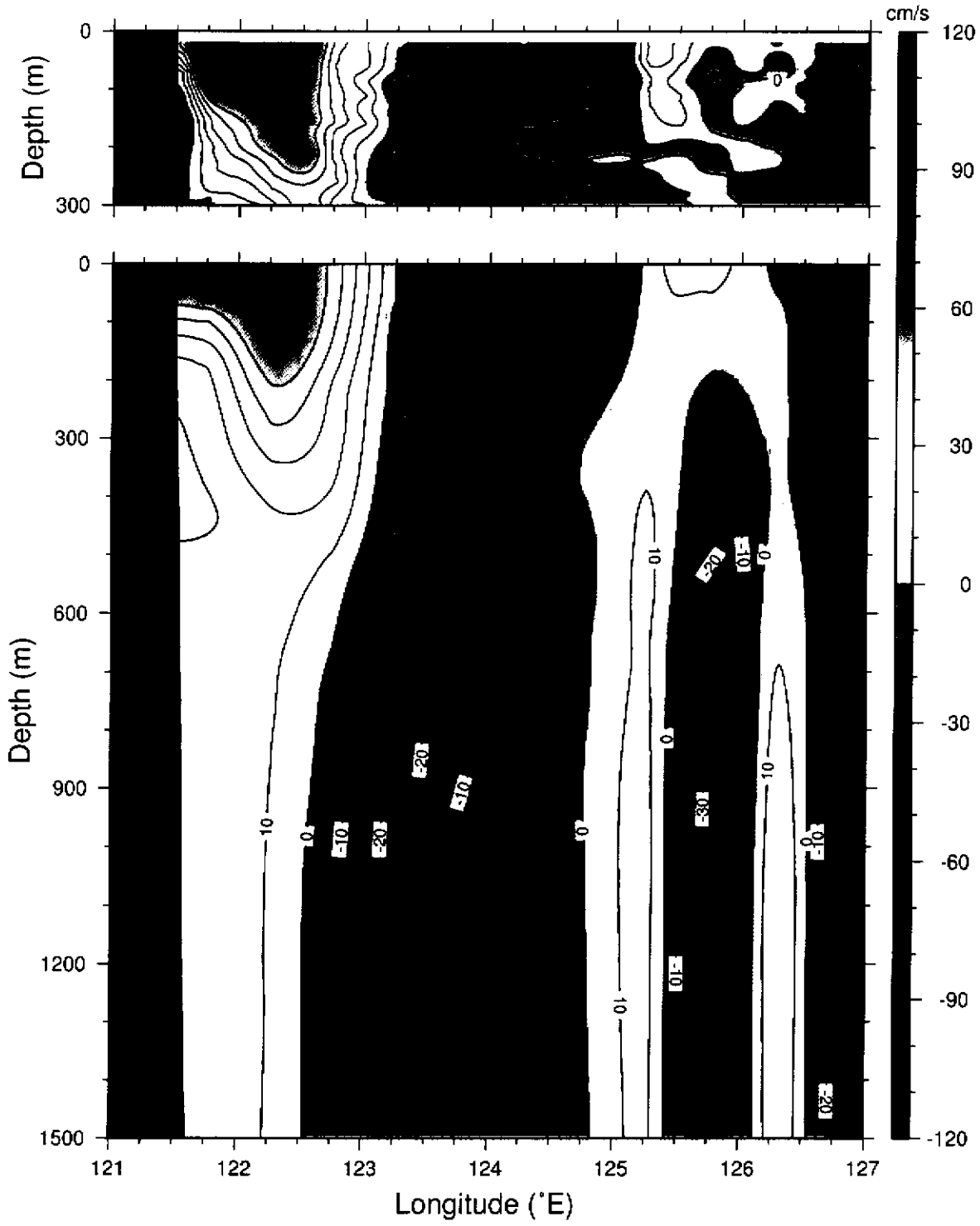

Fig. 3-2

Current Vectors at 16m During Oct 11~16 1999

TOPEX/ERS-2 Analysis Oct 15 1999

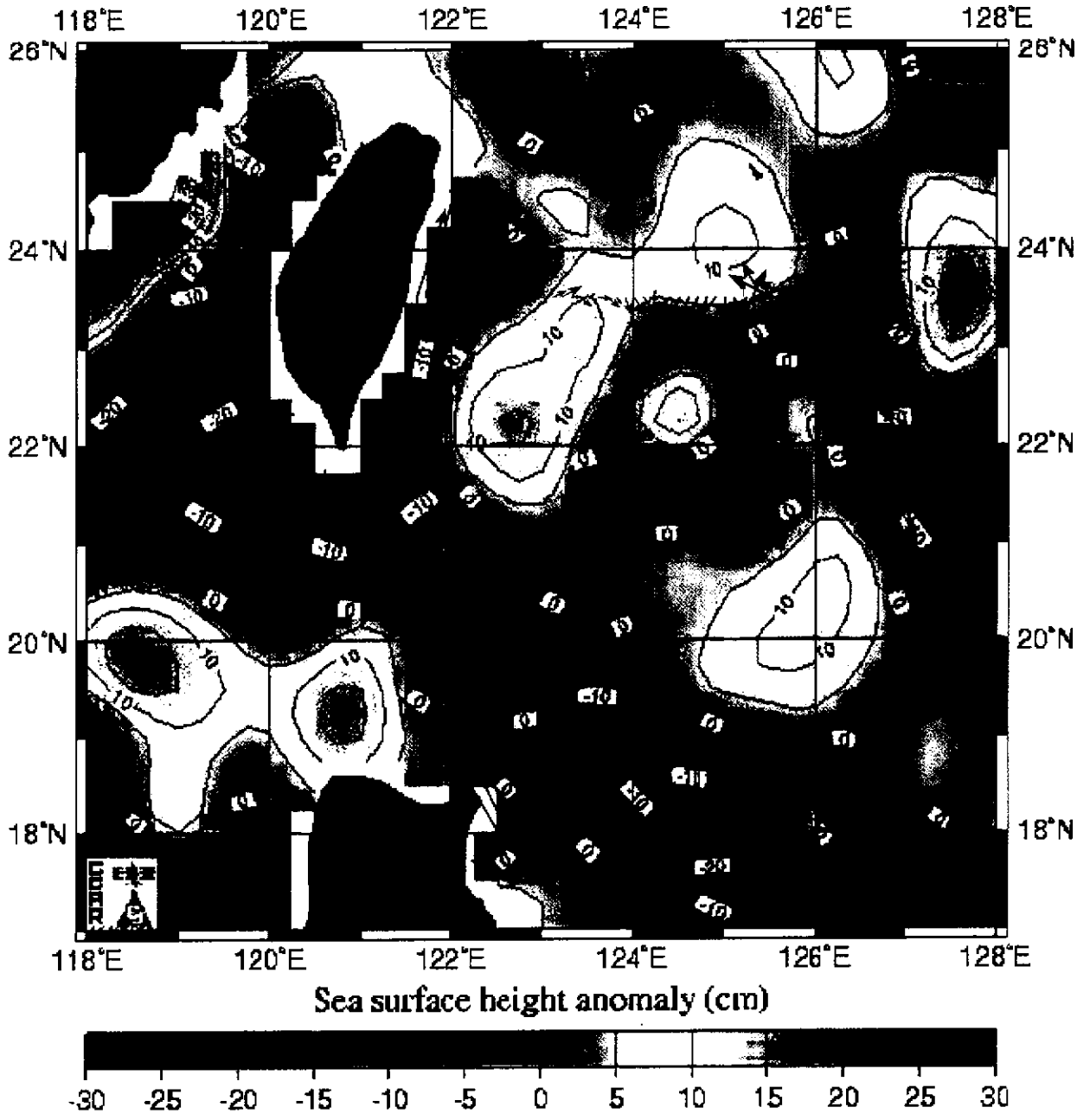

Fig. 3-3

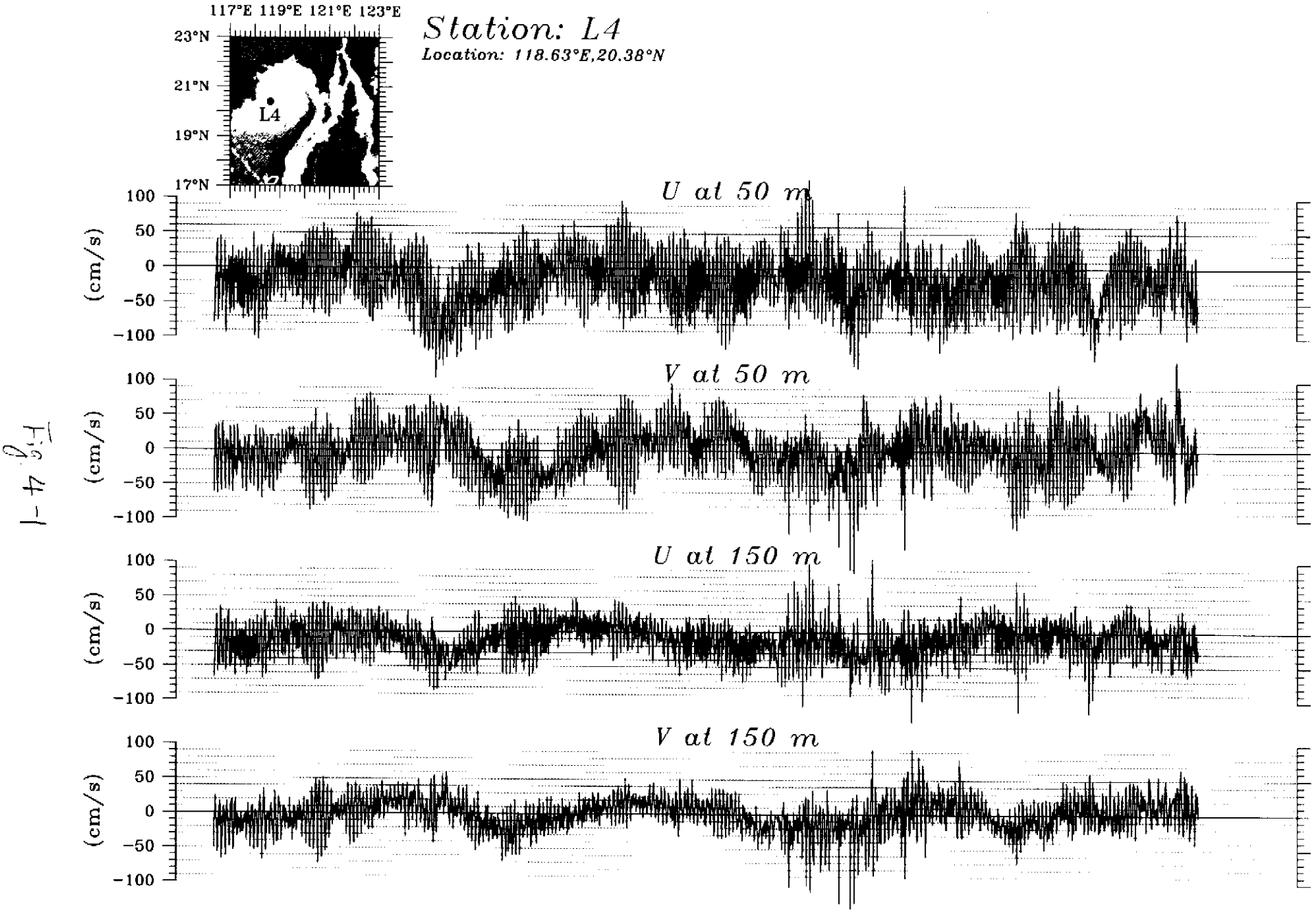
117°E 119°E 121°E 123°E
23°N
21°N
19°N
17°N
L4
Station: L4
Location: 118.63°E,20.38°N
U at 50 m
V at 50 m
U at 150 m
V at 150 m
(cm/s)
100
50
0
−50
−100

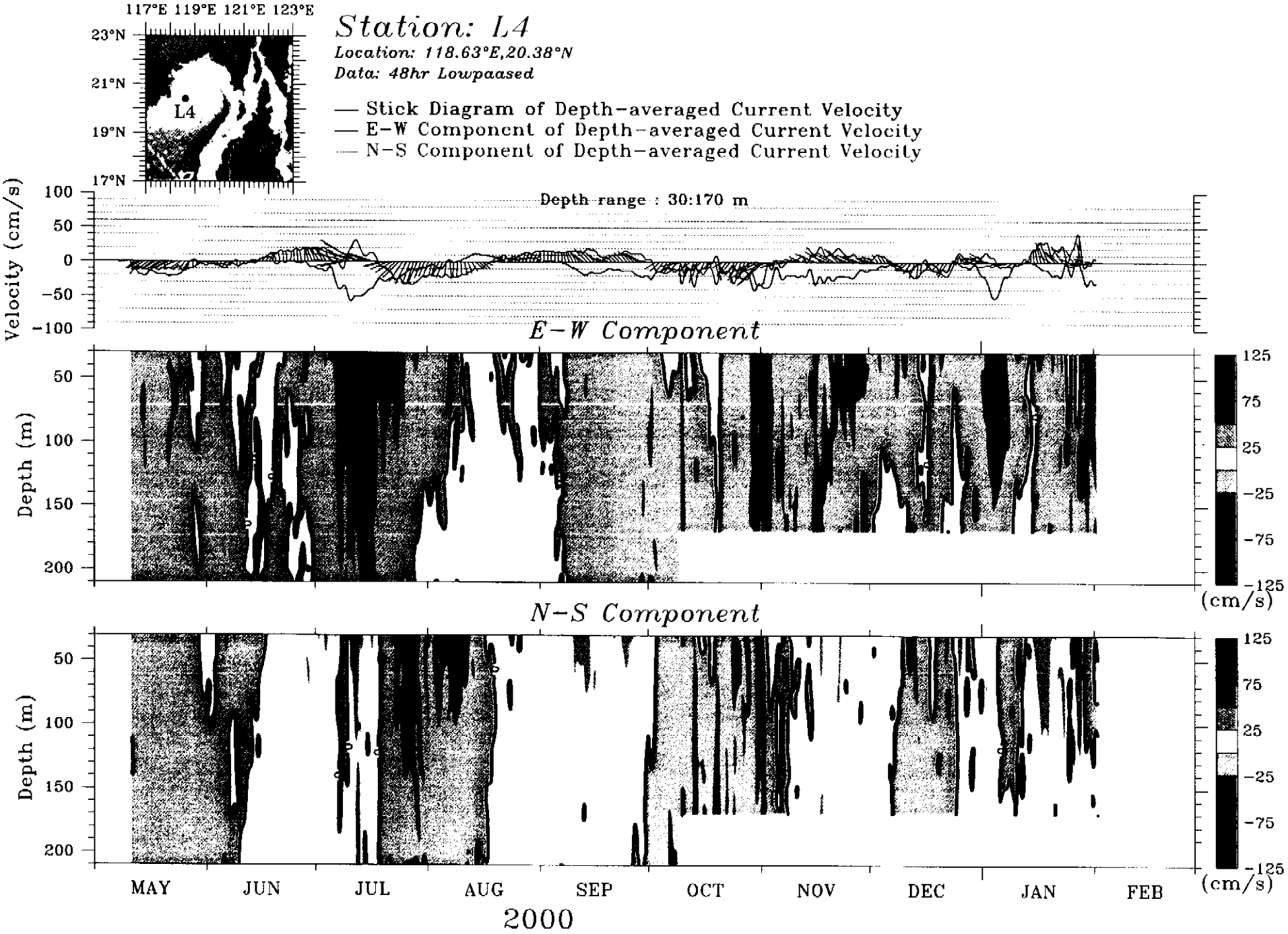
117°E 119°E 121°E 123°E
23°N
21°N
19°N
17°N
L4
Station: L4
Location: 118.63°E,20.38°N
Data: 48hr Lowpaased
— Stick Diagram of Depth-averaged Current Velocity
— E-W Component of Depth-averaged Current Velocity
— N-S Component of Depth-averaged Current Velocity
Depth range : 30:170 m
Velocity (cm/s)
100
50
0
-50
-100
E-W Component
Depth (m)
50
100
150
200
125
75
25
-25
-75
-125
(cm/s)
N-S Component
Depth (m)
50
100
150
200
125
75
25
-25
-75
-125
(cm/s)
MAY
JUN
JUL
AUG
SEP
OCT
NOV
DEC
JAN
FEB
2000

Fig 4-2

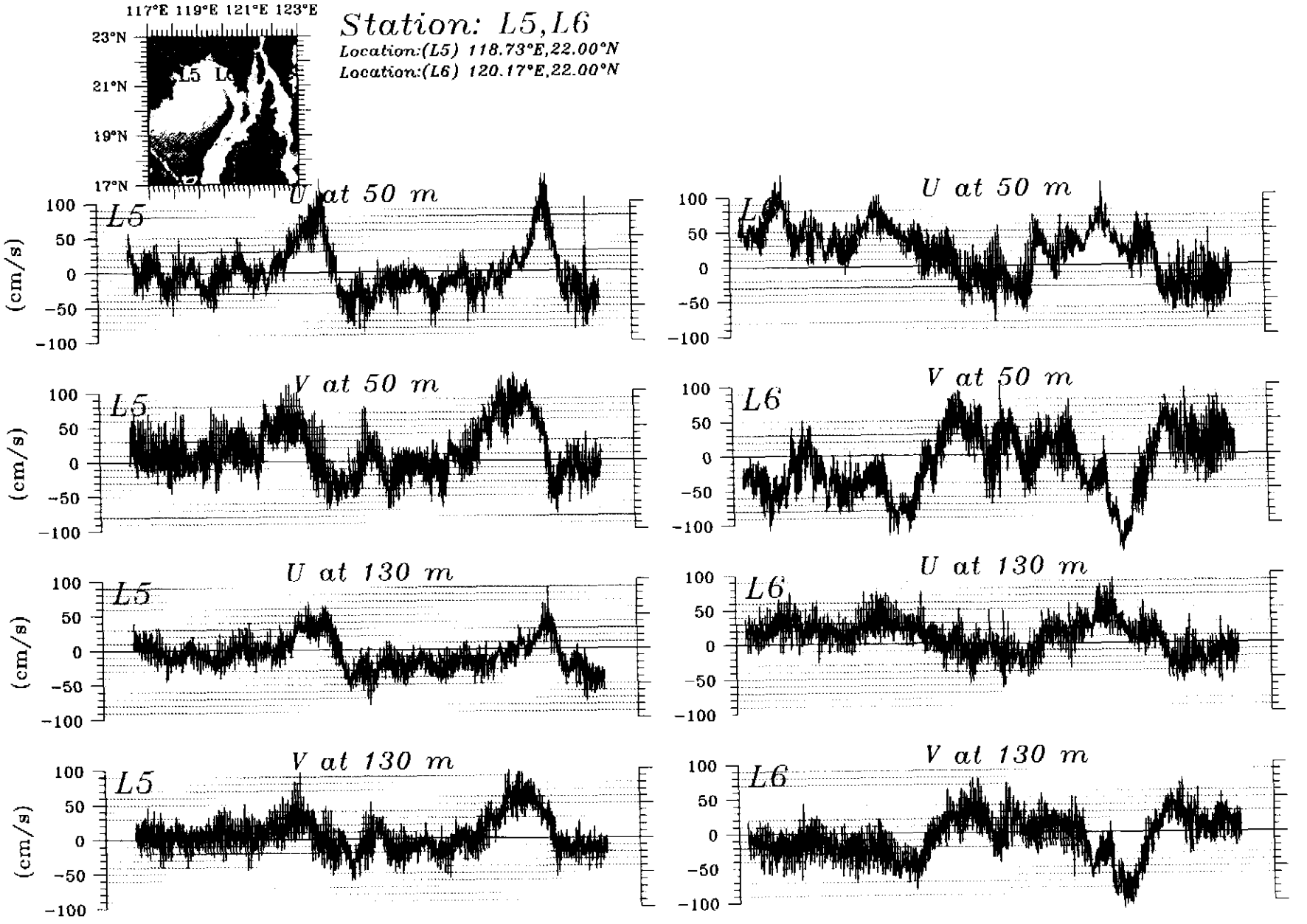
117°E 119°E 121°E 123°E
23°N
21°N
19°N
17°N
L5
Station: L5,L6
Location:(L5) 118.73°E,22.00°N
Location:(L6) 120.17°E,22.00°N
U at 50 m
V at 50 m
U at 130 m
V at 130 m
L6
(cm/s)
100
50
0
-50
-100

Fig 4-3

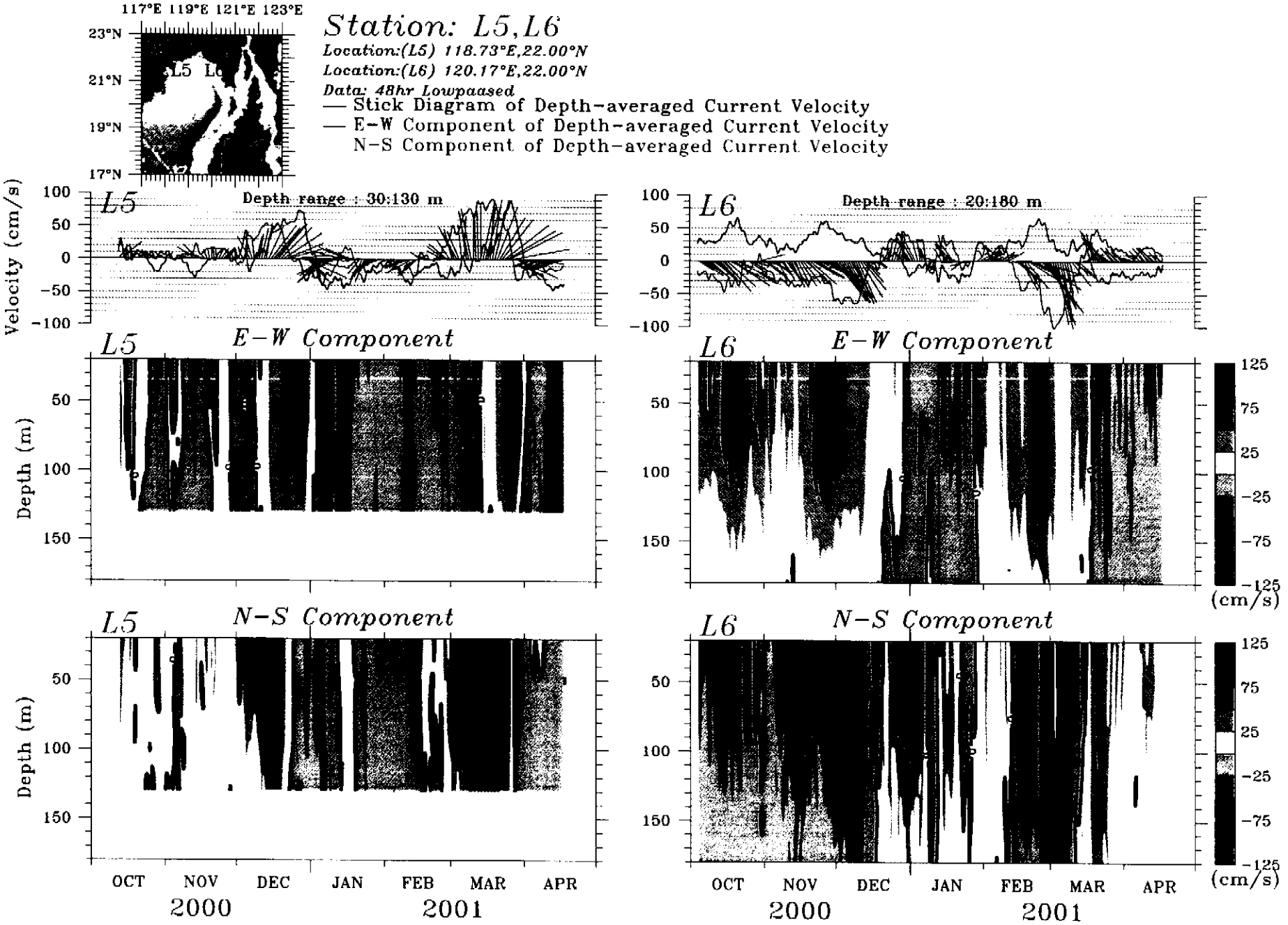
117°E 119°E 121°E 123°E
23°N
21°N
19°N
17°N
L5
Station: L5,L6
Location:(L5) 118.73°E,22.00°N
Location:(L6) 120.17°E,22.00°N
Data: 48hr Lowpaased
— Stick Diagram of Depth-averaged Current Velocity
— E-W Component of Depth-averaged Current Velocity
N-S Component of Depth-averaged Current Velocity
Velocity (cm/s)
100
50
0
-50
-100
L5
Depth range : 30:130 m
L6
Depth range : 20:180 m
E-W Component
Depth (m)
50
100
150
125
75
25
-25
-75
-125
(cm/s)
N-S Component
OCT
NOV
DEC
JAN
FEB
MAR
APR
2000
2001

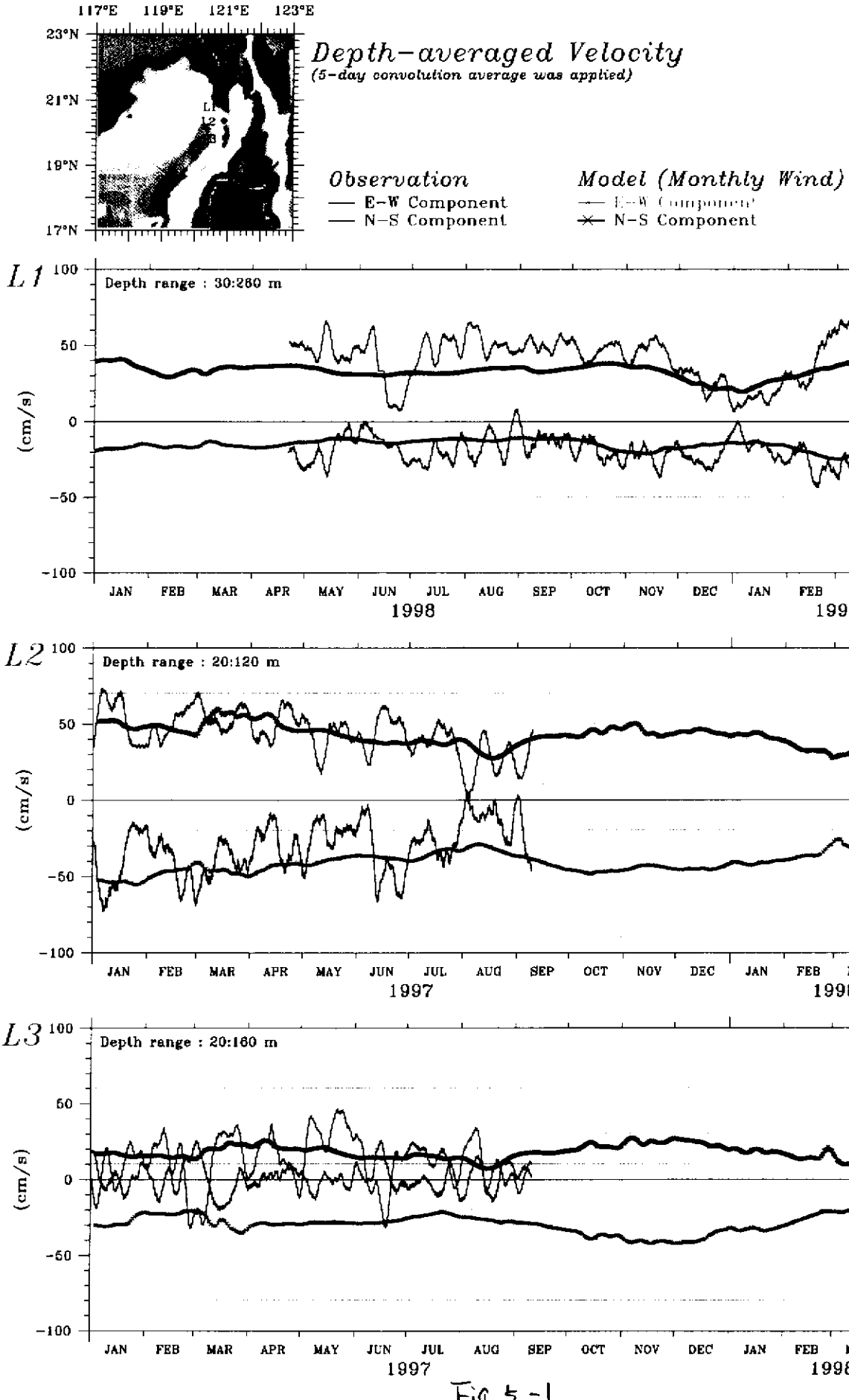
117°E
119°E
121°E
123°E
23°N
21°N
19°N
17°N
Depth-averaged Velocity
(5-day convolution average was applied)
Observation
E-W Component
N-S Component
Model (Monthly Wind)
E-W Component
N-S Component
L1
Depth range : 30:260 m
L2
Depth range : 20:120 m
L3
Depth range : 20:160 m
(cm/s)
100
50
0
-50
-100
JAN
FEB
MAR
APR
MAY
JUN
JUL
AUG
SEP
OCT
NOV
DEC
1998
1999
1997

Fig. 5-1

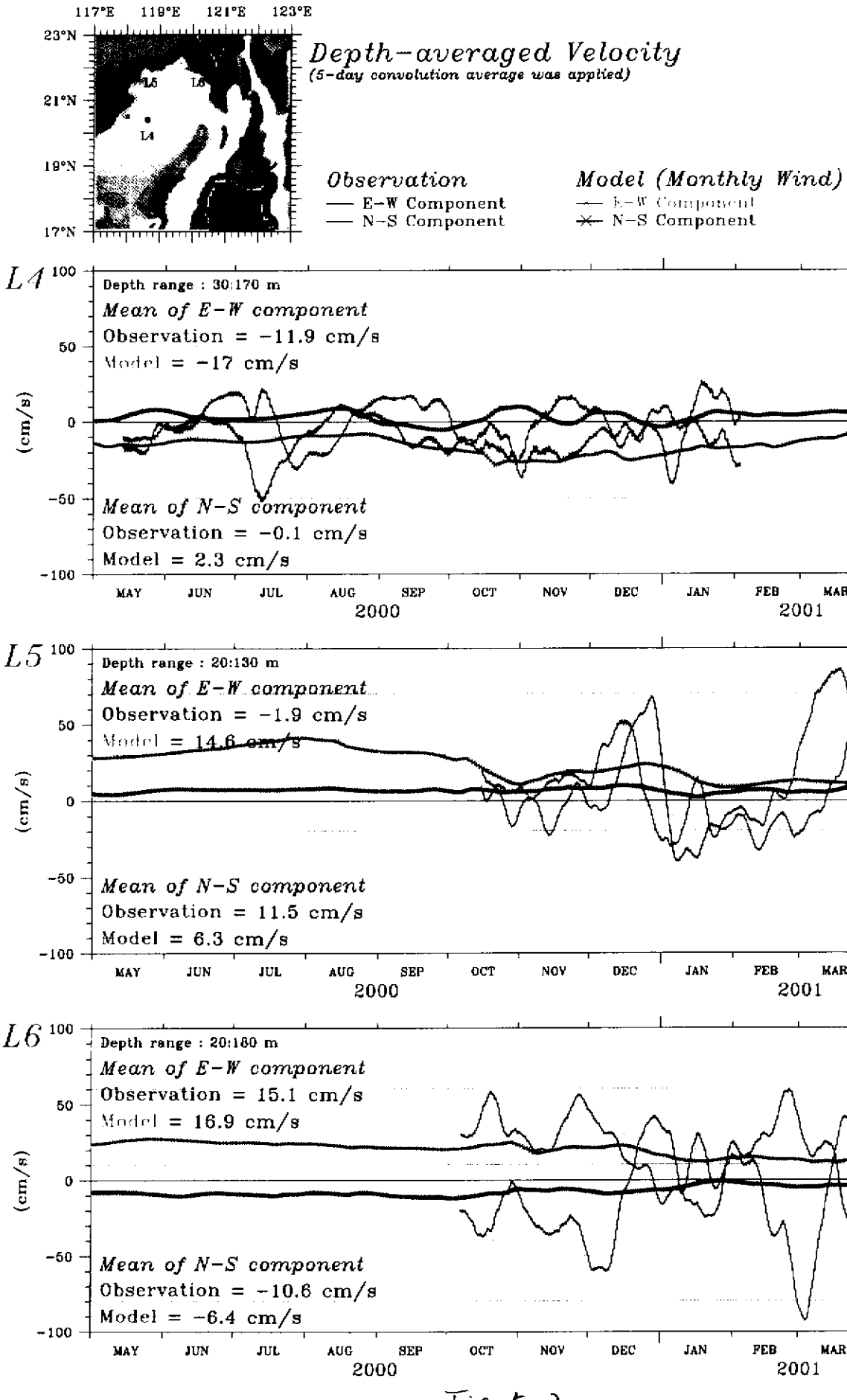
117°E
119°E
121°E
123°E
23°N
21°N
19°N
17°N
L5
L6
L4
Depth-averaged Velocity
(5-day convolution average was applied)
Observation
E-W Component
N-S Component
Model (Monthly Wind)
E-W Component
N-S Component
L4
Depth range : 30:170 m
Mean of E-W component
Observation = -11.9 cm/s
Model = -17 cm/s
Mean of N-S component
Observation = -0.1 cm/s
Model = 2.3 cm/s
L5
Depth range : 20:130 m
Mean of E-W component
Observation = -1.9 cm/s
Model = 14.6 cm/s
Mean of N-S component
Observation = 11.5 cm/s
Model = 6.3 cm/s
L6
Depth range : 20:160 m
Mean of E-W component
Observation = 15.1 cm/s
Model = 16.9 cm/s
Mean of N-S component
Observation = -10.6 cm/s
Model = -6.4 cm/s
(cm/s)
100
50
0
-50
-100
MAY
JUN
JUL
AUG
SEP
OCT
NOV
DEC
JAN
FEB
MAR
APR
2000
2001

Fig. 5-2

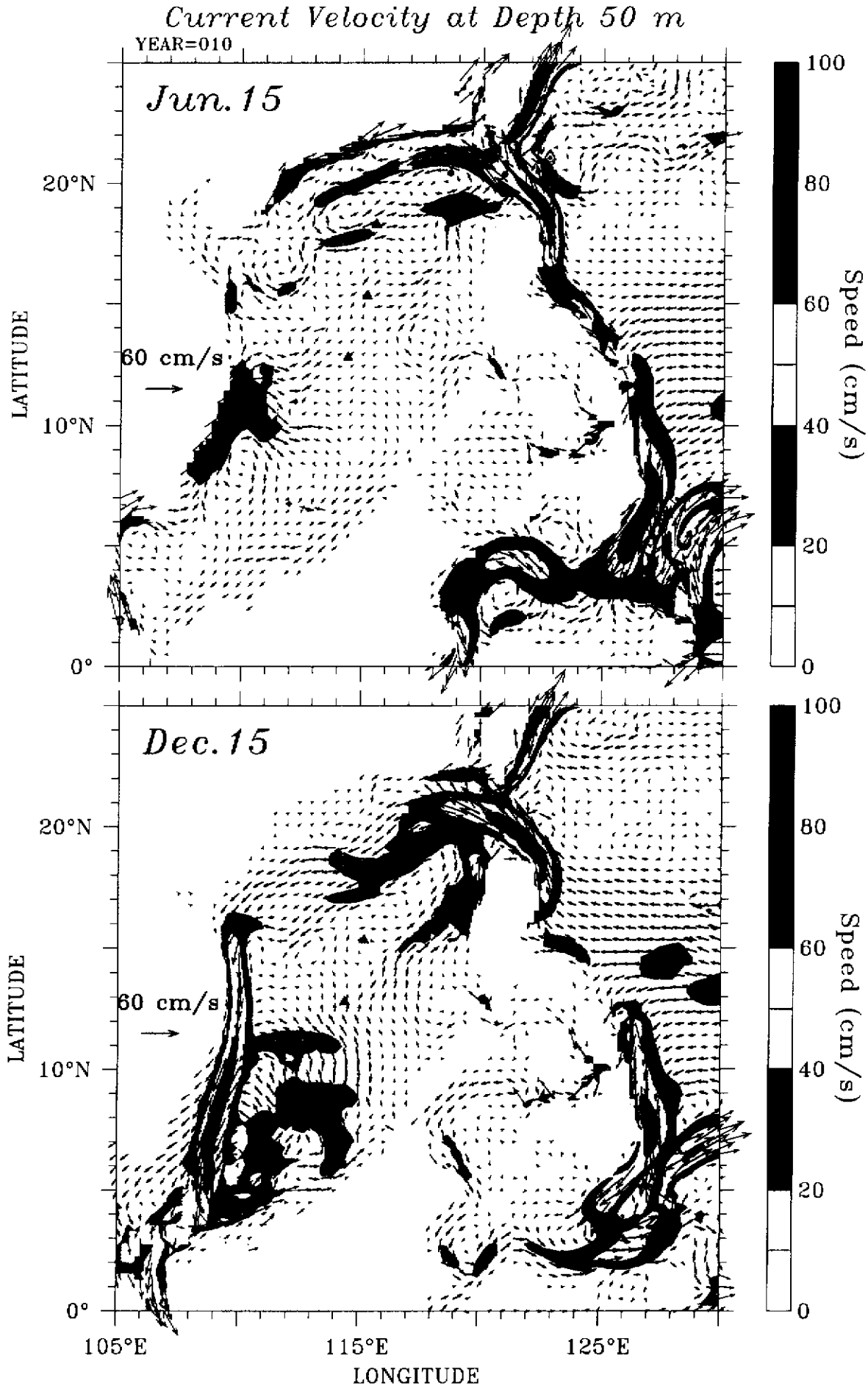
Current Velocity at Depth 50 m
YEAR=010
Jun.15
Dec.15
60 cm/s
60 cm/s
20°N
10°N
0°
LATITUDE
105°E
115°E
125°E
LONGITUDE
100
80
60
40
20
0
Speed (cm/s)

Fig. 6-1

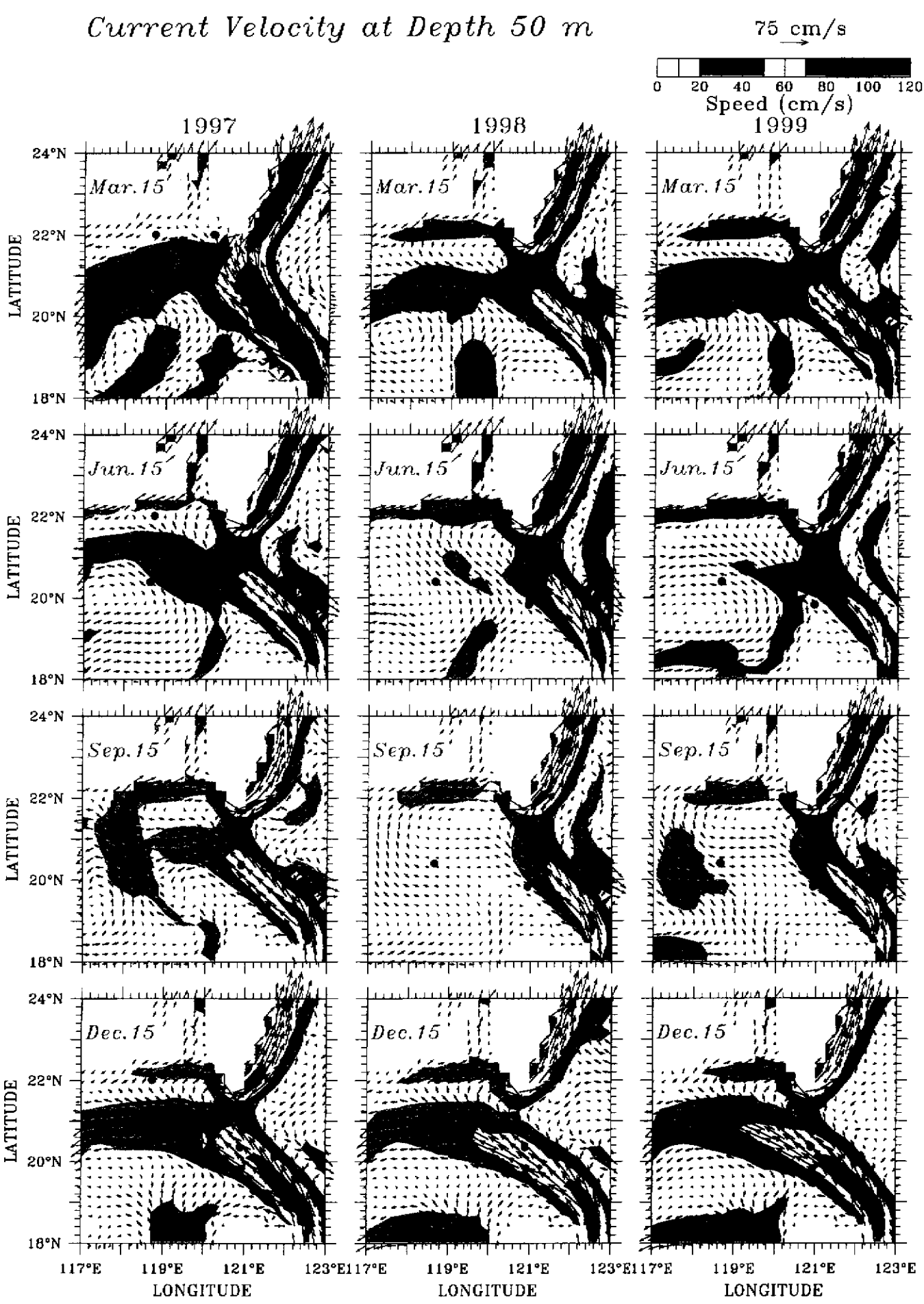
Current Velocity at Depth 50 m
75 cm/s
0 20 40 60 80 100 120
Speed (cm/s)
1997
1998
1999
Mar.15
Jun.15
Sep.15
Dec.15
LATITUDE
LONGITUDE
24°N
22°N
20°N
18°N
117°E
119°E
121°E
123°E

Fig. 6-2

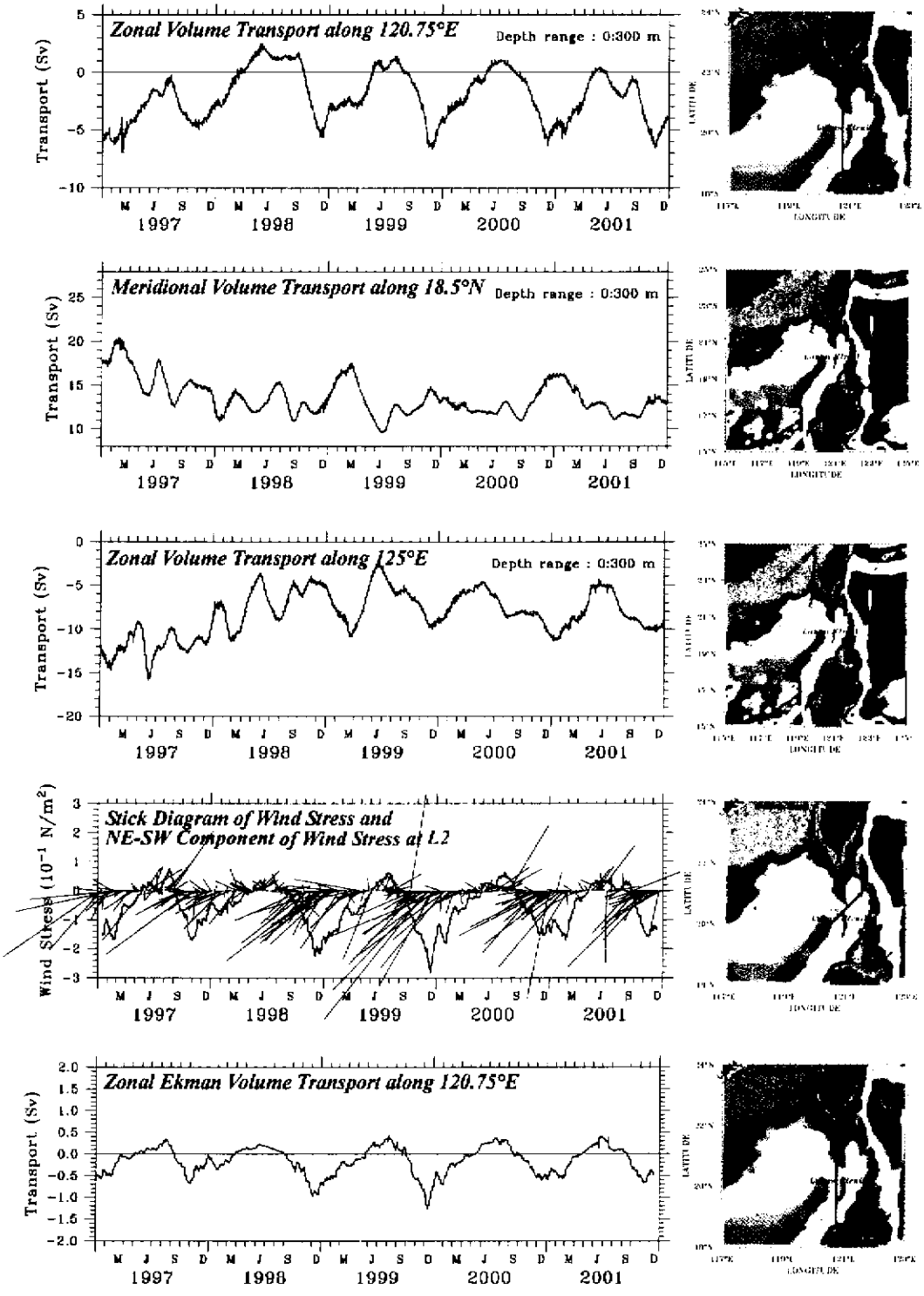
Zonal Volume Transport along 120.75°E
Depth range : 0:300 m
Transport (Sv)
Meridional Volume Transport along 18.5°N
Depth range : 0:300 m
Transport (Sv)
Zonal Volume Transport along 125°E
Depth range : 0:300 m
Transport (Sv)
Stick Diagram of Wind Stress and
NE-SW Component of Wind Stress at L2
Wind Stress (10^{-1} N/m^2)
Zonal Ekman Volume Transport along 120.75°E
Transport (Sv)
M J S D M J S D M J S D M J S D M J S D
1997 1998 1999 2000 2001
LONGITUDE
LATITUDE

Fig. 6-3

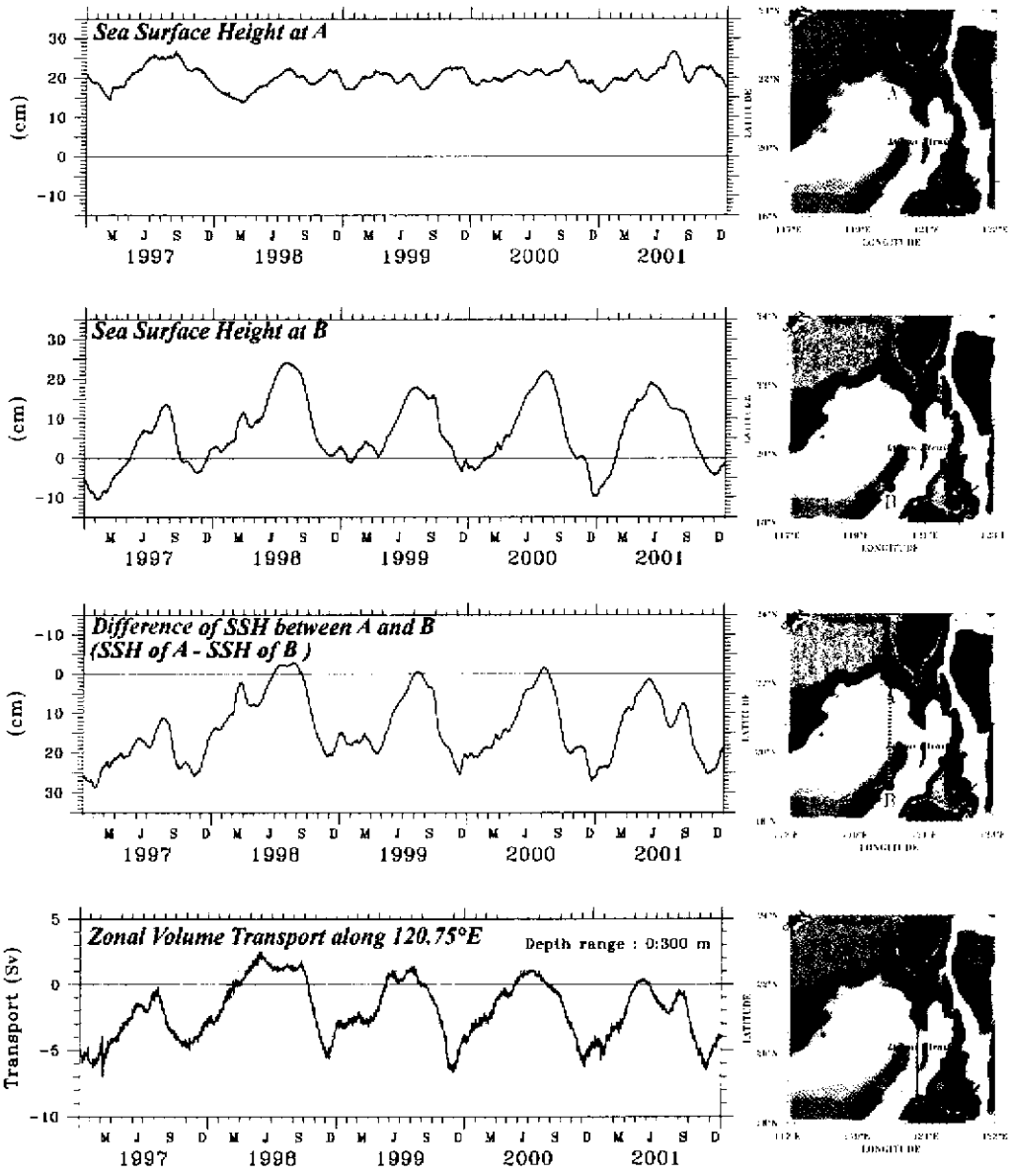
Sea Surface Height at A
(cm)
30
20
10
0
-10
M J S D M J S D M J S D M J S D M J S D
1997
1998
1999
2000
2001
A
Sea Surface Height at B
(cm)
B
Difference of SSH between A and B
(SSH of A - SSH of B)
(cm)
Zonal Volume Transport along 120.75°E
Depth range : 0-300 m
Transport (Sv)
5
0
-5
-10
LATITUDE
LONGITUDE

Fig 6-4

Upper Ocean Current around Taiwan

W.-D. Liang[1], T. Y. Tang[1, 3], Y. J. Yang[2], M. T. Ko[1], and W.-S. Chuang[1]

[1]*Institute of Oceanography, National Taiwan University, Taipei, Taiwan, Republic of China*

[2]*Department of Applied Science, Chinese Naval Academy, Kaohsiung, Taiwan, Republic of China*

[3]*Corresponding Author*

Deep-Sea Research, Part II

(Revised)

March 2002

Abstract

Current velocity, measured by Shipboard Acoustic Doppler Current Profiler (Sb-ADCP) during 1992-2000, was used to study the upper ocean (< 300 m) current around Taiwan. The collected data was debugged, calibrated, grid, and averaged to compose a three-dimensional current velocity distribution. The validity of composite current velocity was supported by twelve sets of moored current velocity time series. Qualitative agreement was obtained. The moored time series also indicated that the seasonal variation of current around Taiwan was generally weak except in the shallow water regimes.

The composite and moored current velocity showed that a branch of Kuroshio intruded steadily and persistently into the South China Sea. A part of the intruded Kuroshio flowed out of the South China Sea through the northern Luzon Strait and re-united with the main stream Kuroshio. East of southern Taiwan, the Kuroshio had two velocity maximum cores, but gradually combined into one as the Kuroshio flowed further north. The Kuroshio was deflected by the I-Lan Ridge east of Taiwan, and deflected again by the zonal-running shelf break northeast of Taiwan. The latter deflection made the Kuroshio split. A portion of Kuroshio intruded into the shelf. The migration of Kuroshio increased the spatial complexity of current northeast of Taiwan.

To the west of the Luzon Strait, the intruded Kuroshio interacted with the South China Sea current flowing westward into the South China Sea. How the westward current collided with the

shelf of the northern South China Sea is unclear. However, a portion of this current flowing along the shelf break, partially intruded into the Taiwan Strait and partially re-poured into the Kuroshio. The current flow in the Taiwan Strait was mostly northward. The southward countercurrent was only found near the coast of Mainland China. North of the Taiwan Strait, the outflow moved primarily northward except for a branch that flowed along the northern coast of Taiwan and joined the Kuroshio.

Composite current velocity differed between seasons in a generally consistent manner. Current velocity usually correlated poorly with the local winds, especially in the deep-water regime. Remote forces may be an important influence on the current around Taiwan.

1. Introduction

Taiwan is an island located in the tropic to sub-tropic western Pacific. Its geographic location and bathymetry are shown in Fig. 1. East of Taiwan, where the shelf is narrow and the water is deep, there are a few islands, including Lan-Yu, Green Island and Yonaguni Island. The I-Lan Ridge connects Yonaguni Island to Taiwan. Northeast of Taiwan, the shelf break extends from the island northeastwardly, but abruptly turns zonally around 26°N. The North Mien-Hwa Canyon stretches across the shelf break around the turning point and connects the shelf of East China Sea with the deep ocean basin. A board shelf exists north of Taiwan. The Taiwan Strait is located between Taiwan and Mainland China and measures 200 km in width, 400 km in length, and 60 m in average depth. A water depth of over 200 m occurs only at the southeastern portion of the Taiwan Strait. The funnel shaped Peng-Hu Channel, which has a wide southern opening, is located between Taiwan and the Peng-Hu Archipelagos. West of Peng-Hu Channel, lies the Taiwan Bank, where the water is very shallow and connects with the northern shelf of the South China Sea. The Luzon Strait, which is located between Taiwan and Luzon, bonds the western Pacific Ocean and the South China Sea together. Its length is around 400 km and its depth varies with the maximum depth of 2000 m occurring near its center. The water is deep on both sides of the Luzon Strait. The topography around Taiwan is generally complex. Swift current such as the

Kuroshio flowing over it could generate intricate temporal and spatial variability.

The monsoon is predominant around Taiwan. In general, the northeasterly and southwesterly monsoons prevail during November-March and May-September, respectively. April and October are the times of transition (Chuang and Liang, 1994). Most previous studies (e.g. Wyrtki, 1961) point to the monsoon as the primary external force causing the variation of current around Taiwan. Nitani (1972) gave the integrated representation for the surface current around Taiwan in summer and winter (see Fig. 2), respectively. The Kuroshio flows along the coast of Taiwan to the north. Leaving Taiwan, it flows along the shelf break of the East China Sea. Through the Luzon Strait, the Kuroshio intrudes into the South China Sea in winter, while the South China Sea water is injected into the Kuroshio in summer. East of Taiwan, the width of the Kuroshio is around 100 km with a maximum speed of around 100 cm s^{-1}. The pathway of the Kuroshio almost parallels the shoreline of Taiwan. The Kuroshio demonstrated no obvious seasonal variation. The current on the shelf northeast of Taiwan flows primarily northeastward regardless of the seasons. North of the Peng-Hu Archipelagos, the current in the Taiwan Strait flowed northeastward in summer and southwestward in winter. South of the Peng-Hu Archipelagos, the current flowed primarily northeastward regardless of the seasons. It is noted that the seasonal difference between the above surface currents in summer and winter is not obvious, except in the Luzon Strait and northern Taiwan Strait.

Many oceanographers believe that the Kuroshio intrudes into the South China Sea through the Luzon Strait in winter and the intrusion of the Kuroshio is halted in summer. This was first described by Wyrtki (1961), and since has been re-confirmed by a number of studies (e. g. Shaw, 1989). There are however, a few studies, e.g. Qu et al. (2000) and Li and Wu (1989), which indicated that the intrusion of Kuroshio also occurs in summer. The potential intrusion of Kuroshio through the Luzon Strait is controversial. Prior studies were largely based upon hydrographic measurement. In this study, the direct current velocity measurement will be provided and the issue of Kuroshio intrusion will be clarified.

Based upon the hydrographic measurement and principal of geostrophy, the width, maximum speed, and transport of Kuroshio east of Taiwan were estimated by a number of earlier studies. Their findings were similar, but contained some notable differences. For example, the transport estimated by Nitani (1972), Chu (1976), and Liu (1983) varied from 19 to 47 Sv. The estimated influence depth of the Kuroshio varied from a few hundred to a thousand meters. Sun (1987) indicated that the main axis of the Kuroshio varied seasonally, especially north of the I-Lan Ridge. The Kuroshio migrated close to the coast in winter and away from the coast in summer. Chu (1976) found that the Kuroshio had no clear annual variation but did have a large interannual variation. Recently the moored current velocity measurement along the I-Lan Ridge and altimetry obtained from the TOPEX/POSEDIENT satellite indicated that the westward propagating eddy from the

Pacific Ocean had a significant impact on the Kuroshio (Yang et al., 1999; Zhang et al., 2001). The transport of Kuroshio displayed a distinguished intra-seasonal variation, with around 100 days time scale, but its annual variation was vague.

Analysis of the moored current velocity, temperature, and salinity time series northeast of Taiwan, Tang et al. (2000) suggests the axis of the pathway of the Kuroshio migrated not only seasonally but also intra-seasonally. Such migration has a great impact on the flow pattern north of Taiwan, where the Kuroshio intrudes onto the shelf and interacts with the Taiwan Strait outflow. A southwestward countercurrent, flowing opposite to the Kuroshio, was observed along the shelf edge northeast of Taiwan (Chuang and Wu, 1991; Tang and Yang, 1993; Chuang et al., 1993). As the Kuroshio moved close to shore, it intruded directly into the shelf along northeastern Taiwan. The northwestward current prevailed in the upper ocean (< 150 m) and the countercurrent was submerged. When the Kuroshio was away from the shore, the Kuroshio intruded onto the shelf mainly through the North Mien-Hwa Canyon. A cyclonic eddy was formed between the North Mien-Hwa Canyon and Taiwan (Tang et al., 1999). The countercurrent surfaced and an annual cycle was completed. Using the Shipboard Acoustic Doppler Current Profiler (Sb-ADCP), Tang et al. (2000) pointed out that the current on the shelf north of Taiwan was primarily northward flowing regardless of season. The impact of monsoon on the current was minimal.

Chu (1961) claimed that the current in Taiwan Strait was dominated by a number of factors,

including the intrusion of the Kuroshio, the South China Sea current, monsoon, and the China coastal current. Wang and Chern (1988) found that the current in the Taiwan Strait was swift and northward under the impact of the southwesterly monsoon in summer, while the Mainland China coastal current flowed southward in the northern Taiwan Strait under the impact of the northeasterly monsoon. The warm and salty Kuroshio met the cold, fresh China coastal water around the central Taiwan Strait. A thermohaline front formed, largely prohibiting the Kuroshio from flowing further north (Wang and Chern, 1989). Chuang (1986) found that the current in the Peng-Hu Channel was northward almost year around. The monsoon had a large impact on the current, but it did not change the current from north to southward, except when the strong northeasterly monsoon retained its strength over an extended period.

This study explores the distribution of three-dimensional upper (< 300 m) ocean current velocity around Taiwan. The current velocity collected during 1992-2000 from the R/Vs Ocean Researcher I, II, and III by the Sb-ADCP is used to obtain the composite current velocity in space. Twelve sets of moored current velocity are used to confirm the validity of composite current velocity and to discuss the temporal variation of the current. This paper will proceed as follows. Section 2 states the edition of the data and gives the composite current velocity distribution around Taiwan. Section 3 discusses how the qualitative validity of composite current velocity and the seasonal variation are confirmed using the moored current velocity measurements. Section 4

investigates the 3-dimensional upper (< 300 m) ocean current velocity around Taiwan using the vertical-meridianal or vertical-zonal sections of current velocity, taking the slices form the composite current velocity. A discussion and summary are provided in Section 5.

2. Data and Composite Current Velocity

The Sb-ADCP measurements used in this study have been provided by the Ocean Data Bank/National Center for Ocean Research (ODB/NCOR) of National Science Council (NSC), Republic of China (ROC). Three Taiwanese research vessels, Ocean Researcher I, II, and III collected the Sb-ADCP measurements from 1992 to 2000. In general, the Sb-ADCP was set to measure the current velocity every second and then to record the ensemble average velocity every 1-2 minutes. The depth bin was 8-16 m and the depth of range of measurement was from 16 to 320 m. The Global Positioning System (GPS) recorded the ship location simultaneous with the current velocity. The ship velocity was then estimated based on the sequential locations. To obtain the composite current velocity, the data was processed as follows. The current velocity was first debugged, calibrated, and aligned using the method described by Tang and Ma (1995). To reduce the random error of estimated ship velocity, which was calculated from the sequential ship

positions recorded by the GPS, a 30-minutes time average was applied. The current velocity was also averaged every 30-minutes. Hereafter, every averaged current velocity is treated as a single data. The mean ship track during that 30-minutes was noted as the location of averaged current velocity. The root mean square (rms) error associated with these calibrated and averaged current velocity was less than ±3.5 cm s^{-1}. Finally, the velocities were linearly interpolated vertically with 10 m intervals and averaged horizontally within the grid of size of 0.25°×0.25°. No further interpolation or smoothing was applied.

Since the Sb-ADCP measurements were not evenly distributed, the numbers of data points in each grid varied. The averaged current velocity in each grid is more representative when there is more data. Conversely, when more data are required within each grid, the obtained composite current velocity distribution becomes more fragmentary. The choice of the minimum requirement of data and integration of composite current velocity has to be confronted. The semidiurnal tidal current could be the primarily high-frequency fluctuation to bias the composite current velocity in each grid. Its possible impact is discussed. The semidiurnal tidal velocity is assumed to be the only high-frequency fluctuation contained in the Sb-ADCP measurements and it has amplitude of 50 cm s^{-1}. To imitate the process of Sb-ADCP data, its 30-mintue average, $\overline{u}$, was calculated. To randomly choose N pieces of $\overline{u}$, its average, $\overline{u}_N$, would be the noise causing the difference between the composite current velocity and true mean current velocity. Theoretically, $\overline{u}_N$ should

decrease as N increases. Finally, to repeat the experiment 100 times, the rms of $\bar{u}_N$ is calculated. The possible error caused by the semidiurnal tidal current in the composite current velocity is estimated. Fig. 3 shows the distribution of numbers of the data, the plot of rms value of $\bar{u}_N$ versus the N, and the available number of grids versus N. The numbers of the data in the grids were distributed unevenly. In general, the grid further away from the Taiwan shoreline had less data. The grids had maximum data in the regions of research vessel harbors, at the northern tip and southwestern tip of Taiwan. The rms value deceases rapidly with N increase initially, but gradually flattens out. The available number of grids also decreases with N increase. To remain the relatively integrated distribution of composite current velocity, N=6 was chosen as the minimum requirement. The estimated bias caused by the semidiurnal tidal current would be 14 cm s^{-1}, around 1/4 of tidal amplitude. Therefore, we limit our description and discussion on the composite current velocity distribution to qualitative comments.

Fig. 4 shows the composite current velocity curved vectors at 30 and 100 m around Taiwan. In general, the current at 30 and 100 m showed no significant difference. North of Luzon, the Kuroshio flowed initially to the northwest, and then gradually turned clockwise, forming a clockwise curve in the Luzon Strait. The main stream of Kuroshio leaped across the Luzon Strait, while portions of the Kuroshio intruded into the northern South China Sea through the northern tip of Luzon, as well as through the central Luzon Strait, where the water is deep. West of northern

Luzon, a branch of the South China Sea current flowed northeastward out of the South China Sea. It gradually turned counterclockwise to the west as it collided with the Kuroshio. The intruded Kuroshio in conjunction with the South China Sea current moved west (seen more clearly at 100 m). The westward current seems to split into two branches after it entered the South China Sea. Perhaps owing to the insufficient data or to the intricate current variation, the southern branch was quite diverse and vague. The resulting numerical model (e.g. Shaw and Chao 1994; Metzger and Hurlburt, 2001; etc) indicates that this southern branch was the main branch. It flowed along the edge of the shelf and penetrated into the central basin of South China Sea. The northern branch was more clearly observed. It turned clockwise, and either re-poured into the Kuroshio through the southern tip of Taiwan or intruded into the Taiwan Strait through the Peng-Hu Channel. A clockwise circulation presented south of Taiwan Strait.

East of Taiwan, the Kuroshio flowed swiftly along the Taiwan coast to the North. Its maximum speed and width were around 100 cm s^{-1} and 100 km, respectively. Over the I-Lan Ridge, the Kuroshio gradually turned northeastward and departed from the coast of Taiwan. Only a small portion of Kuroshio curved, flowing eastward, by the I-Lan Ridge. This finding indicates that the I-Lan Ridge deflected but did not block the Kuroshio. East of the Kuroshio, the data were scarce and does not support any conclusion. The Kuroshio flowed northeastwardly along the shelf break after it leaves Taiwan. Around 26°N, the zonal-running stiff shelf break blocked the

Kuroshio. The Kuroshio then abruptly turned eastward. A part of it spilled over the shelf. On the shelf north of Taiwan, a region (around 25.3°N-25.8°N, 121.7°E-122.2°E) of weak current was observed. A portion of the Taiwan Strait outflow was observed flowing along the northern coast of Taiwan. North of the region of weak current, the current velocity distribution was disorderly and confused. This clutter distribution might be cause by the insufficient data and large bias induced by the large tidal current velocity on the shelf. Tang el al. (2000) claimed that the region of weak current was visional. Because of the seasonal migration of the Kuroshio, the upper (< 150 m) ocean currents were oppositely in that region during the seasons of northeasterly and southwesterly monsoon. Consequently, a weak composite current velocity occurred.

The current in the Taiwan Strait flowed mostly along with the Strait to the north. It originated from the current in the Peng-Hu Channel and the current flowing northeastwardly along the Mainland China coast. The funnel-shaped Peng-Hu Channel converged with the northward current. As the northward current passed over the northern opening of the Peng-Hu Channel, it was blocked by a ridge and separated into two branches. One branch deflected westward, flowing along the topography. The other branch flowed over the local ridge to the north. This feature, current with double peaks crossing the Taiwan Strait, was observed immediately north of the ridge, but became vague further north. A small branch of outflow of Taiwan Strait flowed along the northern coast of Taiwan and poured into the Kuroshio. The main stream of Taiwan Strait outflow

moved continuously to the north, interacting partially with the intruded Kuroshio.

The composite current velocities at 30 m in seasons of southwesterly and northeasterly monsoon are shown in Fig. 5. The former one was similar to the previous velocities distribution. The latter one had less available composite current velocity vectors because the rough sea in the northeasterly monsoon season largely prohibited research vessel activity. In general, the two current velocity distributions were alike. A few notable differences were seen. The Kuroshio primarily leaped across the Luzon Strait during the season of southwesterly monsoon. Only a small potion leaked into the South China Sea. The Kuroshio intrusion in Luzon Strait had a larger incident angle during the season of northeasterly monsoon than during the season of southwesterly monsoon. Northeast of Taiwan, a small cyclonic flow seen on the edge of the shelf (centered around 25.5°N, 122.5°E) was observed during then season of southwesterly monsoon. The cyclonic flow disappeared and the Kuroshio moved close to the shelf when the northeasterly monsoon prevailed. In the Taiwan Strait, the current velocity was weaker in the season of northeasterly than southwesterly monsoon, but it the flow out of the Strait was always directed northeastward. No southward current velocity was clearly observed.

3. Comparison of Moored and Shipboard Current Velocity Measurements

Twelve sets of moored current velocity time series, measured by the self-contained Acoustic Doppler Current Profiler (ADCP) are used to affirm the validity of composite current velocity. The seasonal and intra-seasonal variations of current velocity are noted.

Fig. 6 shows four sets of daily current velocity stick time series at M1, M2, M3, and M4, locations which are shown in Fig. 1. M1 to M3 are in the central portion of Luzon Strait and the M4 is around 230 km west of M2. The current velocity was mostly at 100 m. The 2nd segment at M2 was at 140 m because missed count the rope length of the mooring. The length of the measurement at each site was longer than 5 months. In general, the current velocities at varied depths correlated well in the upper 200 m water column, but their amplitude decreased with the depth. The current velocity at M1 and M2 were essentially northwestward, but M1 was more northward than M2. The transition of monsoons from southwest to northeast, usually occurred in October (Chuang and Liang, 1994), and had little impact on the current velocity. The current at M1 and M2 indicated that the Kuroshio flowed into the South China Sea steadily and persistently. Differing from the current at M1 and M2, the current velocity at M3 was weak and varied frequently from northeastward to northwestward. The current alternated in and out of the South China Sea. The southern boundary of Kuroshio intrusion could be around M3. The current velocity at M4 also was weak and varied, but it only changed its direction from northwest to

southwest. A westward component current velocity was consistently observed. The Kuroshio might intrude further to the west.

The variability and mean of current velocities obtained from the moored and shipboard ADCP at each location were compared (Fig. 7). One diagram contains the 30-minute average Sb-ADCP current velocity in the grid where the mooring occurred, and the other, the hourly moored current velocity. The best agreement was obtained at M1, where the current primarily flowed northwest or north-northwest. The mean moored current velocity vector and composite current velocity are nearly identical. At M2, the moored current velocity primarily flowed northwest while the Sb-ADCP current velocity was more diverse. However, both current velocity directions varied in the same range, from north to west (second quadrant). The mean and composite current velocity vectors had similar direction, but the former one had larger amplitude. Similarly, the two types of measurement at M3 had some similar characteristics but also had notable differences. Both of them showed they were weaker and had more fluctuations than the current at M1 and M2. Considering the difference in the two sampling methods, it is reasonable to conclude that the two types of measurement agreed qualitatively.

Fig. 8 shows the three daily current velocity stick time series. One is located at the I-Lan Ridge and had the shortest record (less than two months). The other two are located at the shelf break northeast of Taiwan. The velocities were at 30 m. At M5, the current was quite stable and

flowed to the north-northeast. A similar observation with much longer time series also showed that the current velocity was generally stable, except when the westward-propagated eddy collided with the Kuroshio. The collision occurred about every 100 days (Yang et al., 1999; Zhang et al., 2001). At M6, the current was first southwestward, and then changed to become northwestward by mid-October. The migration of Kuroshio caused the variation of current velocity. Tang and Yang (1993) and Chuang et al. (1993) described the moored current velocities at M6 in detail. At M7, the current velocity was mainly northeastward, but generally became more eastward in October-April. Tang et al. (2000) claimed the Kuroshio impinged onto the East China Sea shelf around M7. The migration of the Kuroshio also caused the variation of current at M7. However, such variation was not large. In the above three moored current velocities, the large seasonal variation was only seen at M6.

The comparison between the moored and shipboard ADCP current velocity is shown in Fig. 9. In spite of the record being shorter than 2 months, the moored current velocity at M5 agreed well with the shipboard ADCP current velocity in both variability and mean. At M6, the two types of measurement showed a relatively large disparity; though they also had some similarities. Their variability was in the similar range. The mean and composite current velocity vectors had small amplitude and similar direction. The moored and shipboard ADCP current velocity at M7 agreed well in both variability and mean. Generally speaking, the agreement between the two types of

measurement was good when the current velocity variation was small, as occurred at M5. When the current velocity had large fluctuations, as it did at M6, a disparity between the two types of measurement occurred. But overall, the shipboard ADCP current velocity properly represents the current velocity - at least, qualitatively.

Fig. 10 shows the five sets, M8, M9, M10, M11, and M12, daily moored current velocity time series in Taiwan Strait. The velocities were at 30 m. The first four time series were obtained from a mooring array deployed across the Taiwan Strait. The current was observed in the duration of mid-fall to early winter when the northeasterly monsoon prevailed. M12 was located at the southern opening of the Peng-Hu Channel. The current was observed from June--when the southeasterly monsoon prevailed--to November, when the northeasterly monsoon was dominant. In general, the current velocities at M8, M9, M10, and M11 fluctuated considerably with the few days time scale. The coherence between the local wind, which was northeasterly, and current velocity was calculated and generally poor (not shown). At M11, the current flowed even against wind for most of the observed period. However, the impact of local wind on the current velocity was still seen by peak-to-peak comparison. The current velocity at M12 primarily flowed with wind moving toward the southwest. The coherences between the current velocities at various stations were also poor. The above result implies that the local wind was not the only dominant external force in the Taiwan Strait. Remote force, such as the intruded Kuroshio, could play an

import role. At M12, the current velocity persistently flowed into the Peng-Hu Channel, whether the local wind was southwesterly or northeasterly. The northeasterly monsoon, which intensified after October, only caused the current velocity fluctuation. Again, the local wind poorly correlated with the current velocity. The former inference was reconfirmed: Both remote and local forces were important in the Taiwan Strait.

The comparison between the moored and Sb-ADCP current velocities in the Taiwan Strait is shown in Fig. 11. Strong agreement between the two types of measurement was found at M11 and M12. At M8, M9, and M10, a large disparity was observed. The disparity could arise from a number of factors. For example, the data were sparse, especially in the western Taiwan Strait. The Sb-ADCP data were lacking when the northeasterly monsoon was large. There was no moored current velocity in the southwesterly monsoon season. The large semidiurnal tidal current velocity could also be a source of error for the composite current velocity.

The composite current velocity might inadequately represent the current where there was a large current velocity variation. However, this type of current is limited around Taiwan. The above comparison between moored and Sb-ADCP current velocity indicates that the composite current velocity obtained from the Sb-ADCP measurements represents the current around Taiwan qualitatively, but not quantitatively.

4. Vertical Sections of Current Velocity

Fig. 12 shows the vertical sections of zonal (U) and meridional (V) components of current velocity along the Luzon Strait and along 21°N. The blank region indicates where the data was insufficient. The latitude-vertical section of U along the Luzon Strait showed that the eastward/westward current velocity alternately occurred from northern Luzon to southern Taiwan. The westward current occupied a larger area and had larger amplitude than the eastward current. The largest westward current occurred in the central-northern Luzon Strait, while the largest eastward current appeared at the southern tip of Taiwan. The northward current dominated in the V section. Its maximum speed was over 50 cm s^{-1}. The southward current was only observed at the tips of northern Luzon and southern Taiwan. The westward current, indicating that the water intruded into the South China Sea from Pacific Ocean, generally accompanied the large northward current. The intruded current should primarily be the Kuroshio. The South China Sea outflow at southern Luzon Strait could retroflex back to the South China Sea though the central Luzon Strait, but its amount was small. The zonal volume transport, calculated by simply integrating the U along the section, was around -3 Sv. westwardly. Smaller, but also negative, value was obtained by using the Sb-ADCP measurement collected only in the season of southwest monsoon.

Apparently, the Kuroshio intruded into the South China Sea even in the southwest monsoon season. Although the transport of Kuroshio intrusion was only estimated qualitatively, the moored current velocity supported such inference because the Kuroshio intrusion occurred persistently. The earlier belief that no Kuroshio intrusion occurred in the Luzon Strait in summer might need to be reconsidered.

Along 21°N, the longitude-vertical section of U was primarily westward of the Luzon Strait signifying that the intruded Kuroshio flowed continuously westward. The maximum westward speed was around 30 cm s^{-1}. East of the Luzon Strait, the U was fragmented, with eastward/westward current reciprocally shown. The northward current dominated in the V section. A weak southward current was observed west of 119°E. East of this southward current, the northward current extended from 119°E to 121.75°E. The region was wide - around 300 km. The maximum northward current, around 60 cm s^{-1}, was in the Luzon Strait. East of this northward current, the V was negative/positive reciprocally. The Kuroshio became vague around Luzon Strait, possibly because the western boundary current is deficient in its western continental boundary. Local topography might also play a role. A few islands, which nearly falling along the 122°E parallel with the Luzon Strait, might cause the spatial current fluctuation east of Luzon Strait.

East of Taiwan, four longitude-vertical current velocity sections along 22°N, 23°N, 24°N,

and 25°N are shown in Fig. 13. The Kuroshio dominated all four sections. On the most southern section (along 22°N), the U was weak. It was primarily positive (eastward) between Taiwan and Lan-Yu near 121.5°E. East of Lan-Yu, the U gradually turned to negative (westward). A weak eastward component velocity was seen again east of 124°N. The V was chiefly positive (northward) and had two maximum velocity cores located on two sides of Lan-Yu, respectively. The western core with maximum speed over 90 cm s^{-1} was near the surface. The eastern core with maximum speed around 70 cm s^{-1} was at subsurface (70 m). The eastward current generally accompanied the western core while the westward current accompanied the eastern core. This implies that the two cores eventually combined together as the Kuroshio flowed further north. The feature of double maximum velocity cores could be caused by the local topography or the fact that the split Kuroshio in the Luzon Strait had not fully re-united. The southwestward countercurrent was observed close to Taiwan at subsurface as well as east of Kuroshio.

The velocity section along 23°N was similar to it along 22°N. The Kuroshio had double velocity cores. The western core had greater speed and was at surface, while the eastern core had smaller speed and was at subsurface. Again, the cores seem to merge further north. The subsurface countercurrent close to Taiwan was barely observed. West of the Kuroshio, the countercurrent was weaker than that at the section of 22°N.

The two velocity cores merged into a single velocity core at the section of 24°N, south of

I-Lan Ridge. The U and V were mostly positive, but the V has much greater amplitude. The negative U and V were only seen at subsurface close to Taiwan. The Kuroshio was mainly northward; its eastward component was small. I-Lan Ridge is quite close to the section of 24°N, but its impact on the Kuroshio was not observed here.

The velocity at section of 25°N, north of I-Lan Ridge, showed that the U and V were still primarily positive but the amplitude of U increased and the amplitude of V decreased. This result indicates that the Kuroshio was deflected as it flowed over the I-Lan Ridge. The countercurrent was observed close to Taiwan. Its southward component velocity extended to the surface indicating the Kuroshio departed from Taiwan coast. Such separation could be due to the deflection of Kuroshio. Using the similar data, Tang et al. (2000) found that the Kuroshio migrated seasonally, but the migration was small.

Fig. 14 shows the width, main axis, and upper ocean (< 300 m) northward volume transport of Kuroshio. The 10 cm s^{-1} isotach of northward velocity was used as an indicator for the boundaries of the Kuroshio. The maximum northward speed defined the main axis of the Kuroshio. The linear integration was applied to estimate the northward volume transport. From south to north, the main axis of the Kuroshio was close to the coast of Taiwan south of I-Lan Ridge. It departed from the coast as it flowed over the I-Lan Ridge. The maximum speed along the main axis of the Kuroshio showed little variation. It was over 100 cm s^{-1}. The width of the Kuroshio

was around 170 km, but narrowed to 120 km on I-Lan Ridge. The northward volume transport of Kuroshio demonstrated no significant and systematic change south of I-Lan Ridge. It reduced as the Kuroshio approached and flowed over the I-Lan Ridge. The reduction of the northward transport of Kuroshio was essentially caused by deflection of Kuroshio. A part of northward transport turned to eastward transport. The values of northward volume transport are listed as a reference only since the composite current velocity might be inappropriate to make a quantitative estimate. However, the present estimated volume transport in the I-Lan Ridge agreed well with the transport estimated by Johns et al. (2001), whose estimate was obtained from an array of moored current velocity time series.

In summary, the Kuroshio flowed primarily northward along the eastern coast of Taiwan. East of southern Taiwan, the Kuroshio split, but gradually re-united. As the Kuroshio flowed over the I-Lan Ridge, it was deflected eastwardly. The velocity became more eastward. The Kuroshio departed from the Taiwan coast. A subsurface countercurrent close to the island was consistently observed. It surfaced north of I-Lan Ridge.

Since the previous studies indicated that the current along the shelf break northeast of Taiwan had noticeable seasonal variations, Fig. 15 shows the U and V sections along 25.5°N in the seasons of southwesterly and northeasterly monsoon. The seasonal variation was observed. Regardless of the seasons, a negative U occurred around shelf break. It clearly separated the main stream of

Kuroshio and the current on the shelf. Corresponding to this negative U, the V was positive and negative in the upper and lower water column, respectively. However, this distribution of V varied seasonally. The negative V occurred in the deep water in the northeasterly monsoon season, but it extended upwardly to near surface in the southwesterly monsoon season. This result agrees with the earlier finding (Tang et al., 2000) that the subsurface southwestward countercurrent at the shelf break northeast of Taiwan was submerged when the northeasterly monsoon intensified. East of the countercurrent, both U and V were positive. The northeastward Kuroshio was presented and showed much more complicated spatial velocity distribution than it did east of Taiwan. The locations of maximum velocity cores of U and V were different, implying that the Kuroshio was branching. The influence of the zonal-running shelf break north of this section on the Kuroshio was noted. A part of Kuroshio in the upper ocean flowed northward or even northwestward intruding onto the shelf. The shelf blocked the subsurface Kuroshio, which flowed northeastward or even eastward. The Kuroshio also varied significantly with monsoons. In the southwesterly monsoon season, the Kuroshio was weak and its maximum speed core was at subsurface. In the northeasterly monsoon, the weak Kuroshio intensified and the subsurface core nearly disappeared. However, the feature of the Kuroshio having greater speed in winter than summer could be meaningless if we give consideration to the seasonal migration. When the Kuroshio moved away from the shore in southwesterly monsoon season, it may be that only a portion of Kuroshio was

observed. Such migration also caused more Kuroshio intrusion northwestwardly onto the shelf in northeasterly monsoon season.

On the shelf north of Taiwan, the current was generally complicated. The complicated flow distribution could be related to the intrusion of Kuroshio, Taiwan Strait outflow, and their interaction. However, the large semidiurnal tidal current velocity on the shelf could result in a large error in the computed composite current velocity. Such error could further increase the complication of current velocity distribution. Therefore, there is no detailed description of the spatial current velocity distribution on the shelf. Nevertheless, the current on the shelf seems to prefer flowing northeastward regardless of season. The local wind could not be the only dominant force on the shelf north of Taiwan.

Fig. 16 shows four velocity vertical sections along 22°N, 23°N, 24°N, and 25°N in the Taiwan Strait. On the southern opening of Taiwan Strait (section along 22°N), the V was positive and negative in the western and eastern portions, respectively, while the positive U dominated nearly the entire section. This type of velocity distribution supports the former finding, a clockwise circulation south of Taiwan Strait. In the Peng-Hu Channel, the current velocity was mainly northward in the deep channel where the U was weak. West of the deep channel, the U was positive and had relatively simple distribution. The V varied from positive to negative and then to positive again. A couple of maximum speed cores were near bottom. The Peng-Hu Archipelagos

north of this section could be responsible for this complicated flow distribution. However, the net northward transport was positive, indicating that the water flowed into the Taiwan Strait. Along the section of 24°N, the U was negative at the shallow end of the funnel-shaped Peng-Hu Channel, which curved northwestward. It was positive at two sides of the end. The V was primarily positive, except in the region close to Mainland China. The region's large V and negative U nearly coincided, indicating that the Peng-Hu Channel conducted the water flow into the Taiwan Strait. Near the northern opening of the Taiwan Strait (section of 25°N), both U and V were principally positive. Their negative values were seen in the region close to Mainland China. Two regions demonstrated relatively large velocity. One was close to the Taiwan coast. The other one was near the bottom east of Wu-Chiu Island. West of Wu-Chiu Island, a weak southwestward current was observed.

5. Discussion and Summary

Generally speaking, the Kuroshio around Taiwan demonstrated moderate temporal variation, but had complicated spatial distribution, especially around Luzon Strait and northeast of Taiwan.

The spatial complication was caused primarily by the local topography. Ignoring variation caused by the westward propagating eddy, the observed current velocity at I-Lan Ridge (Johns et al., 2001) did not vary with time significantly. The feature of Kuroshio had small temporal fluctuations also occurred in the moored current velocity in Luzon Strait. This result implies that the Kuroshio around Taiwan might be stable in time. In contrast to the velocity, the Kuroshio migrated intra-seasonally and seasonally. The seasonal migration was especially obvious north of I-Lan Ridge. Such seasonal migration caused the large temporal variation in the moored current velocity at shelf break northeast of Taiwan.

Because of insufficient data, the seasonal current velocity distributions along the sections were almost not presented. Rough seas frequently prohibited the activities of research vessels in winter. The Sb-ADCP data were less in the northeasterly than the southwesterly monsoon seasons. Inevitably, the composite current velocity was biased. It more favorably represented the current velocity distribution in the southwesterly monsoon season. Even so, the moored current velocity showed the current around Taiwan generally had little seasonal variation, especially in the deep-water region. Even in the shallow regions such as Taiwan Strait, the composite current velocity vectors had similar tendencies to the mean moored current velocity vectors, which were only obtained from the duration of large northeasterly monsoon. Therefore, the bias could not significantly change the distribution of composite current velocity.

In summary, the composite current velocity, obtained from the Sb-ADCP, was used to study the three-dimensional upper (< 300 m) ocean current velocity around Taiwan. The qualitative, but not quantitative, validity of composite current velocity was supported by twelve sets of moored current velocity. The results showed that the Kuroshio intruded into the South China Sea through the northern-central Luzon Strait regardless of season, but its incident angle could vary with season. The Kuroshio with double velocity cores was seen east of southern Taiwan, but the two cores gradually combined into one before the I-Lan Ridge. The I-Lan Ridge deflected the Kuroshio. The Kuroshio branched as it collided with the zonal-running shelf break northeast of Taiwan. The main stream of the Kuroshio flowed along the shelf break to the east and a part of the Kuroshio intruded into the shelf. A countercurrent between the Kuroshio and the Taiwan coast or between the Kuroshio and the shelf break was consistently observed. It was generally submerged. The seasonal migration of Kuroshio had an influence on the countercurrent and the current northeast of Taiwan.

The intruded Kuroshio in the South China Sea interacted with the South China Sea current. The flow pattern shown in the composite current velocity was indistinct. However, a clockwise flow pattern was seen southwest of Taiwan. Most of this clockwise current injected into the Kuroshio at the tip of southern Taiwan. The rest of it flowed into the Taiwan Strait through the Peng-Hu Channel. It could be the important resource for current in the Taiwan Strait. The current

in the Taiwan Strait primarily flowed to the north. A countercurrent was faintly visible along the coast of Mainland China. The Taiwan Strait outflow interacted with the intruded Kuroshio north of Taiwan. Only a small portion of outflow flowed along the northern coast of Taiwan pouring into the Kuroshio. The rest of outflow continuously flowed to the north.

Although the current velocity around Taiwan varied lightly with the seasons, its spatially seasonal distribution should be further studied. Therefore, the Sb-ADCP measurements should be continuously collected and edited.

Acknowledgements

The research was supported by NSC of ROC under grants NSC 89-2611-M-002-031-OP2 for T. Y. Tang, NSC 90-2611-M-012-001-OP2 for Y. J. Yang, and NSC 89-2611-M-002-023-OP2 for W.-S. Chuang. We would like to express our heartfelt thanks to the ODB/NCOR for the historical Sb-ADCP and bathymetry data. The assistance of the captains and crews of the R/Vs ORI, II, and III are also greatly appreciated. The plotting software of curved velocity vectors was kindly provided by Dr. D. S. Ko at Naval Research Laboratory, Stennis Space Center (NRLSSC).

References

Chu T.-Y. (1961) On ocean currents in East China Sea and the Variability of Taiwan. *Meteorological Bulletin*, **4**, 7-17. (in Chinese with English abstract)

Chu T.-Y. (1976) Study of the Kuroshio current between the Taiwan and Ishigakijima. *Acta Oceanographic Taiwanica*, **13**, 140-153.

Chuang W.-S. (1986) A note on the driving mechanisms of current in the Taiwan Strait. *Journal of Oceanography Society Japan*, **42**, 355-361.

Chuang W.-S., and C.-K. Wu (1991) Slope-current fluctuation northeast of Taiwan, winter 1990. *Journal of Oceanography Society Japan*, **47**, 185-193.

Chuang W.-S., H.-W. Li, T. Y. Tang and C.-K. Wu (1993) Observation of the countercurrent on the inshore side of the Kuroshio northeast of Taiwan. *Journal of Oceanography*, **49**, 581-592.

Chuang W.-S. and W. D. Liang (1994) Seasonal variability of intrusion of the Kuroshio water across the continental shelf northeast of Taiwan. *Journal of Oceanography*, 50, 531-542.

Johns W. E., T. N. Lee, D. Zhang, R. Zantopp, C.-T. Liu and Y. Yang (2001) The Kuroshio east of Taiwan: Moored transport observations from the WOCE PCM-1 array. *Journal of Physical Oceanography*, **31**, 1031-1053.

Li L. and B. Wu (1989) A Kuroshio loop in South China Sea? On circulation of the northeaster South China Sea. *Journal of Oceanography in Taiwan Strait*, **8**, 89-95.

Liu C.-T. (1983) As the Kuroshio turns: (I) Characteristics of the current. *Acta Oceanographic Taiwanica*, **14**, 88-95.

Megtzger E. J. and H. E. Hurlburt (2001) The nondeterministic nature of Kuroshio penetration and eddy shedding in the South China Sea. *Journal of Physical Oceanography*, **31**, 1712-1732.

Nitani H. (1972) Beginning of the Kuroshio. In: *Kuroshio, its physical aspects*, H. Stommel and K. Yoshida, editors, University of Tokyo Press, Tokyo, pp. 129-163.

Qu T., H. Mitsudera and T. Yamagata (2000) Instruction of the North Pacific waters into the South China Sea. *Journal Geophysical Research*, **105**, 6415-6424.

Shaw P.-T. (1989) The instruction of water masses into the sea southwest of Taiwan. *Journal Geophysical Research*, **94**, 18,213-18,226.

Shaw P.-T. and S.-Y. Chao (1994) Surface circulation in the South China Sea. *Deep-Sea Research*, **41**, 1663-1683.

Sun X. (1987) Analysis of the surface path of the Kuroshio in the East China Sea. In: *Essays of the Investigation of Kuroshio*, X. Sun, editor, Ocean Press, Beijing, pp. 1-14 (in Chinese with

English Abstract).

Tang T. Y. and Y. J. Yang (1993) Low frequency current variability on the shelf break northeast of Taiwan. *Journal of Oceanography*, **49**, 193-210.

Tang T. Y. and J. C. Ma (1995) A note on the accuracy of shipboard ADCP on Ocean Researcher I. *Acta Oceanographic Taiwanica*, **34**, 71-81.

Tang T. Y., Y. Hsueh, Y. J. Yang and J. C. Ma (1999) Continental slope flow northeast of Taiwan. *Journal of Physical Oceanography*, **29**, 1353-1362.

Tang T. Y., J. H. Tai and Y. J. Yang (2000) The flow pattern north of Taiwan and migration of the Kuroshio. *Continental Shelf Research*, **20**, 349-371.

Wang J. and C.-S. Chern (1988) On the Kuroshio branch in the Taiwan Strait during wintertime. *Progress in Oceanography*, **21**, 469-491.

Wang J. and C.-S. Chern (1989) On cold water instructions in the eastern Taiwan Strait during the cold season. *Acta Oceanographic Taiwanica*, **21**, 469-491.

Wyrtki K. (1961) *Physical oceanography of the southeast Asia waters*. Scripps Institute of Oceanography NAGA Report, **2**, 195 pp.

Yang Y., C.-T. Liu, J.-H. Hu and M. Koga (1999) Taiwan Current (Kuroshio) and impinging eddies.

Journal of Oceanography, **55**, 609-617.

Zhang D., T. N. Lee, W. E. Johns, C.-T. Liu and R. Zantopp (2001) The Kuroshio east of Taiwan: Modes of variability and relationship to interior ocean mesoscale eddies. *Journal of Physical Oceanography*, **31**, 1054-1074.

Figure Captions

Fig. 1. Bathymetric chart showing areas around Taiwan and mooring locations.

Fig. 2. Current charts in knots: (a) summer, and (b) winter (after Nitani, 1972).

Fig. 3. The left panel denotes the distribution of numbers of data. The right-upper and right-lower panels represent the root mean square (rms) value of the $\overline{u}_N$, and the available percentage of grid versus the N, respectively.

Fig. 4. Composite of the Sb-ADCP current velocity vectors around Taiwan. The left and right panels represent the 30 and 100 m depths, respectively.

Fig. 5. Composite of the Sb-ADCP current velocity vectors at 30 m depths around Taiwan. The left and right panels represent the seasons of southwesterly monsoon and northeasterly monsoon, respectively.

Fig. 6. The stick diagrams of the 36-hour low-pass filtered current velocity. The upper to lower panels represent the time series data of M1 in 1997, 1998, and 1999, M2 in 1997 and 1998, M3 in 1997, and M4 in 2000. The current velocity data was primarily at 100 m depths except the M2 in 1998, which was at 140 m depths.

Fig. 7. The rose diagrams and mean current velocities obtained from shipboard and moored

ADCP measurement at M1, M2, M3, and M4. The left, central, and right panels represent the rose diagrams of the shipboard and moored ADCP data, and the mean velocities, respectively. The range of rose is 0-30% with 7.5% interval.

Fig. 8. The stick diagrams of the 36-hour low-pass filtered current velocity. The upper to lower panels represent the time series data of M5 in 1992, M6 in 1991, and M7 in 1992, 1993, and 1994. The current velocity data was at a depth of 30 m.

Fig. 9. Same as Fig. 7 except at M5, M6, and M7. The range of rose is 0-60% with 15% interval.

Fig. 10. The stick diagrams of the 36-hour low-pass filtered current velocity. The upper to lower panels represent the time series data of M8, M9, M10, and M11 in 1999, and M12 in 1996. The current velocity data was at a depth of 30 m.

Fig. 11. Same as Fig. 9 except at M8, M9, M10, M11, and M12.

Fig. 12. Vertical sections of composite Sb-ADCP current velocity of zonal (U) and meridional (V) components along the 120.75°E and 21°N are show in left and right panels, respectively. The depth range is from the surface to about 300 m. The continental shelf is darkened. The values are contoured at intervals of 10 cm s^{-1}. The zero contour appears in heavy line. Portions of positive values are shaded.

Fig. 13. Vertical sections of composite Sb-ADCP current velocity of zonal (U) and meridional (V) components along the 22°N, 23°N, 24°N, 25°N east of Taiwan are show in left and right panels, respectively. The depth range is from the surface to about 300 m. The continental shelf is darkened. The values are contoured at intervals of 10 cm s^{-1}. The zero contour appears in heavy line. Portions of positive values are shaded.

Fig. 14. The upper ocean (< 300 m) northward volume transport of Kuroshio and composite Sb-ADCP current velocity vectors at 30 m depths east of Taiwan. Bold and dashed lines indicate the width and main axis of Kuroshio.

Fig. 15. Vertical sections of composite Sb-ADCP current velocity of zonal (U) and meridional (V) components along the 25.5°N in seasons of southwesterly monsoon and northeasterly monsoon are show in left and right panels, respectively. The depth range is from the surface to about 300 m. The continental shelf is darkened. The values are contoured at intervals of 10 cm s^{-1}. The zero contour appears in heavy line. Portions of positive values are shaded.

Fig. 16. Same as Fig. 13 except in Taiwan Strait.

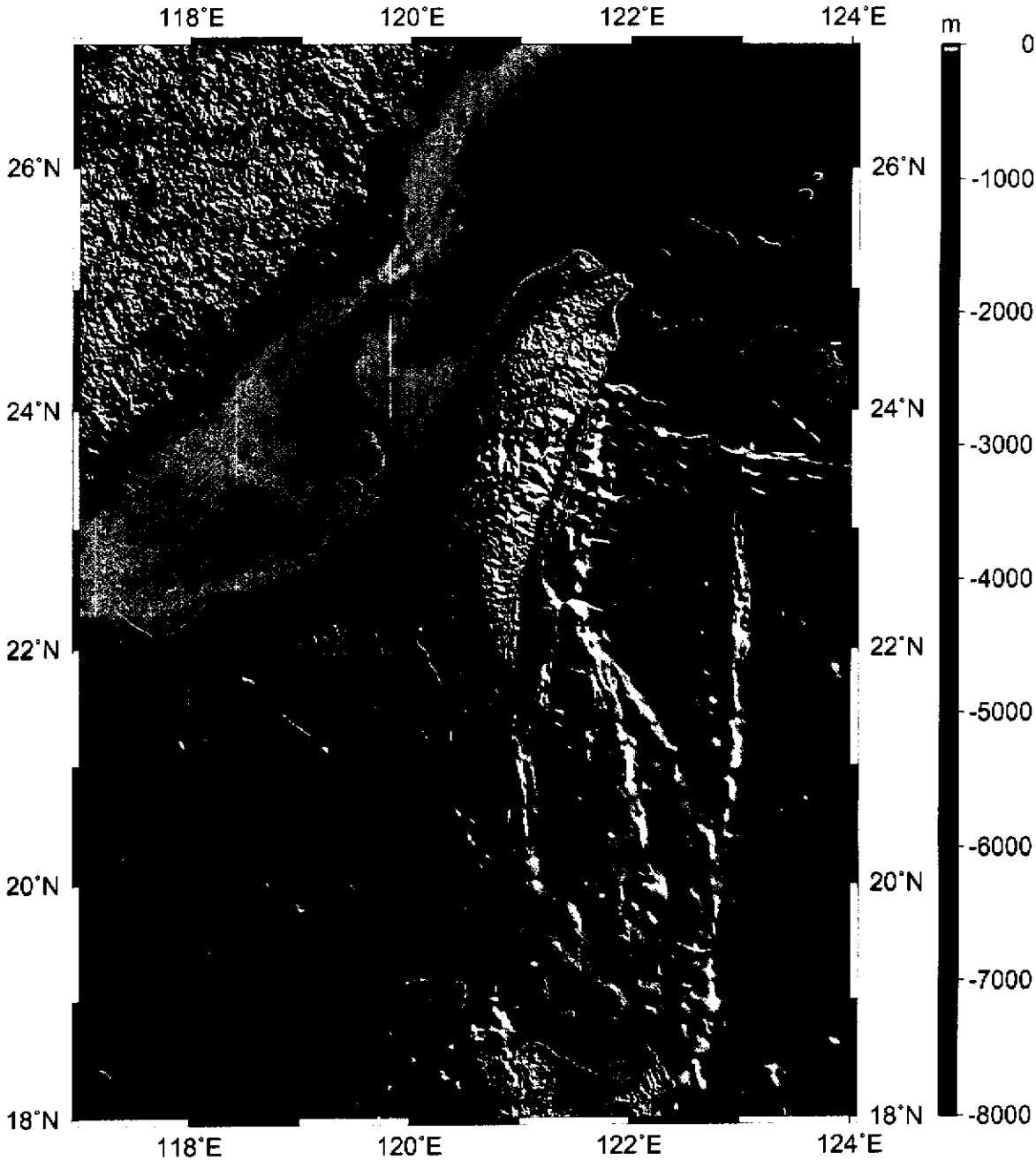
118°E
120°E
122°E
124°E
26°N
24°N
22°N
20°N
18°N
m
0
-1000
-2000
-3000
-4000
-5000
-6000
-7000
-8000

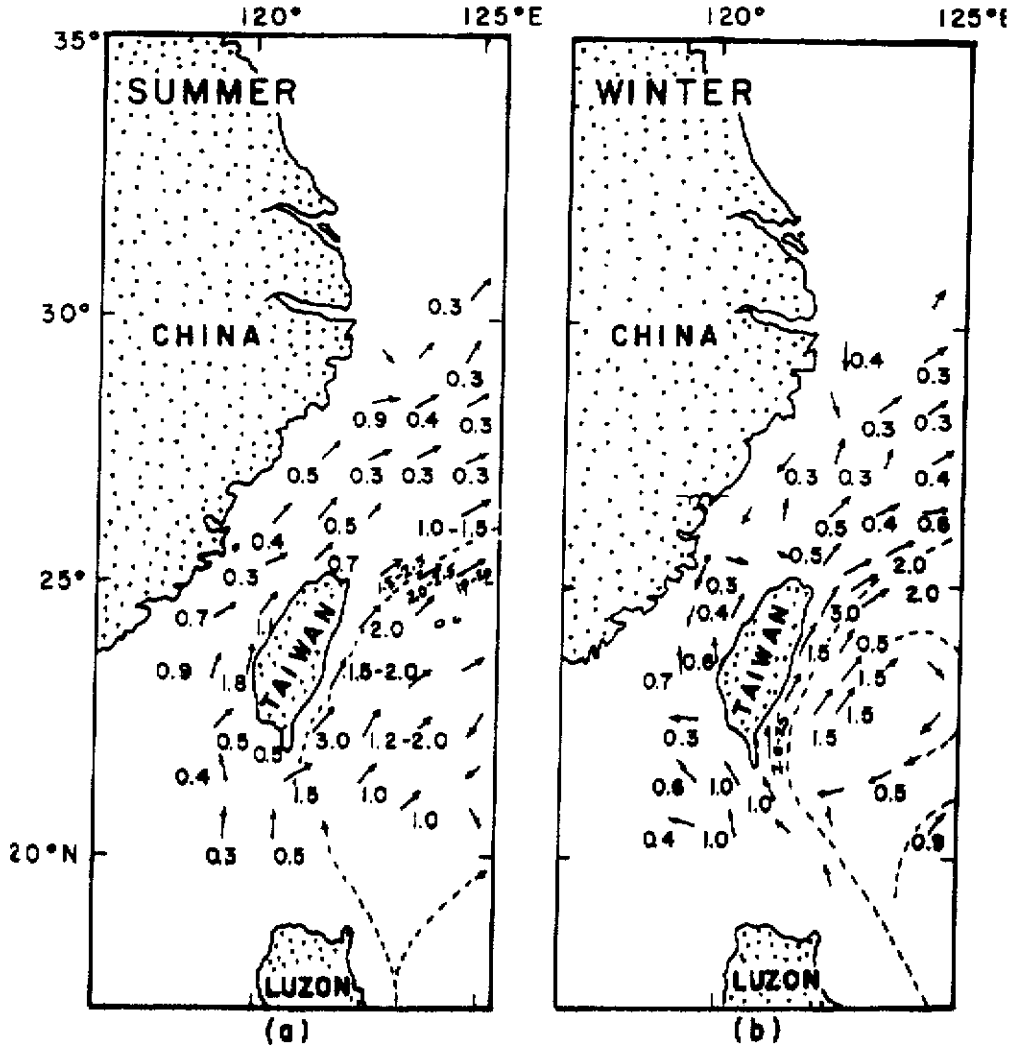
120°
125°E
35°
30°
25°
20°N
SUMMER
CHINA
TAIWAN
LUZON
(a)
WINTER
CHINA
TAIWAN
LUZON
(b)

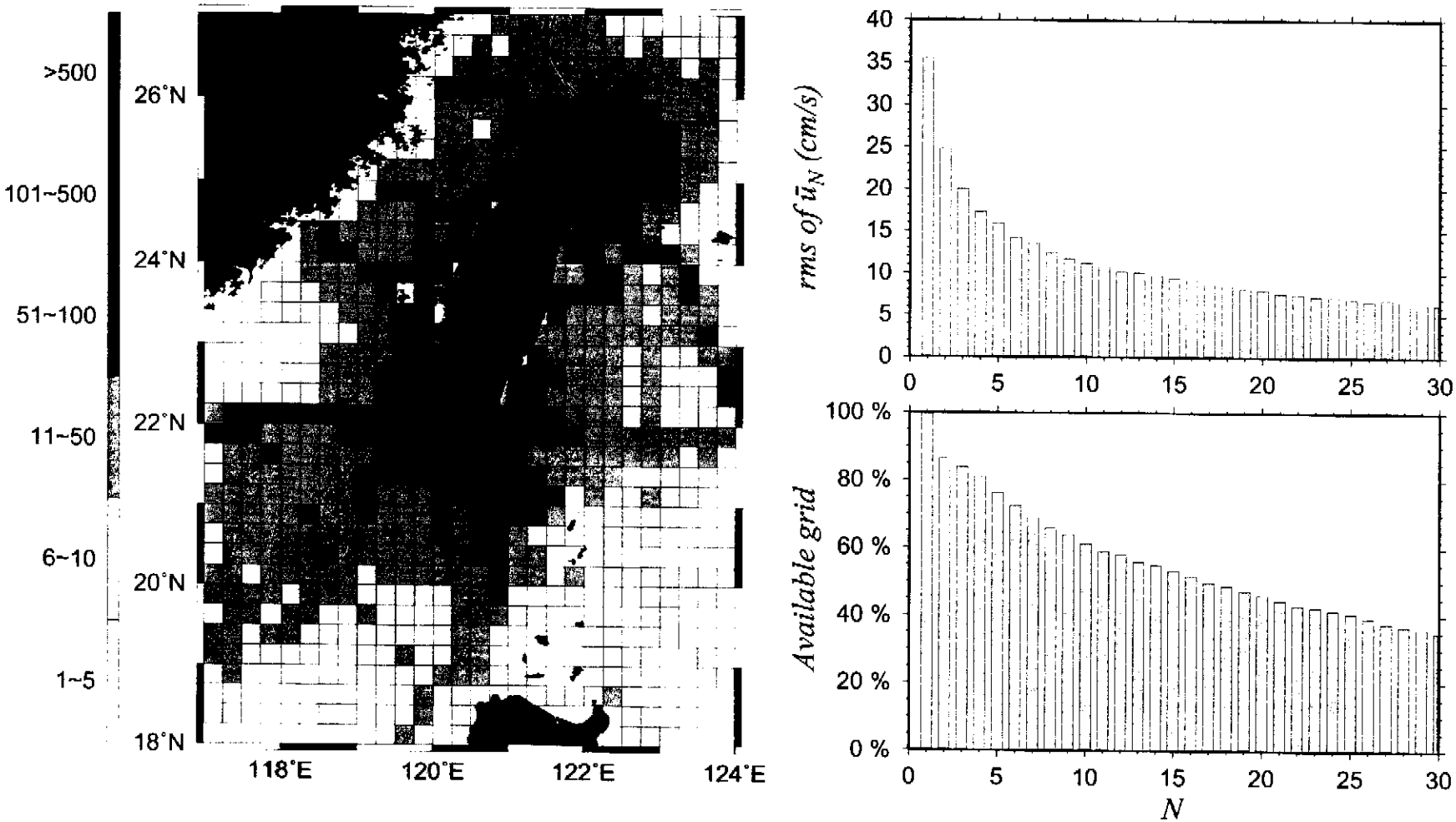
>500
101~500
51~100
11~50
6~10
1~5
26°N
24°N
22°N
20°N
18°N
118°E
120°E
122°E
124°E
rms of $\bar{u}_N$ (cm/s)
40
35
30
25
20
15
10
5
0
0
5
10
15
20
25
30
Available grid
100 %
80 %
60 %
40 %
20 %
0 %
N

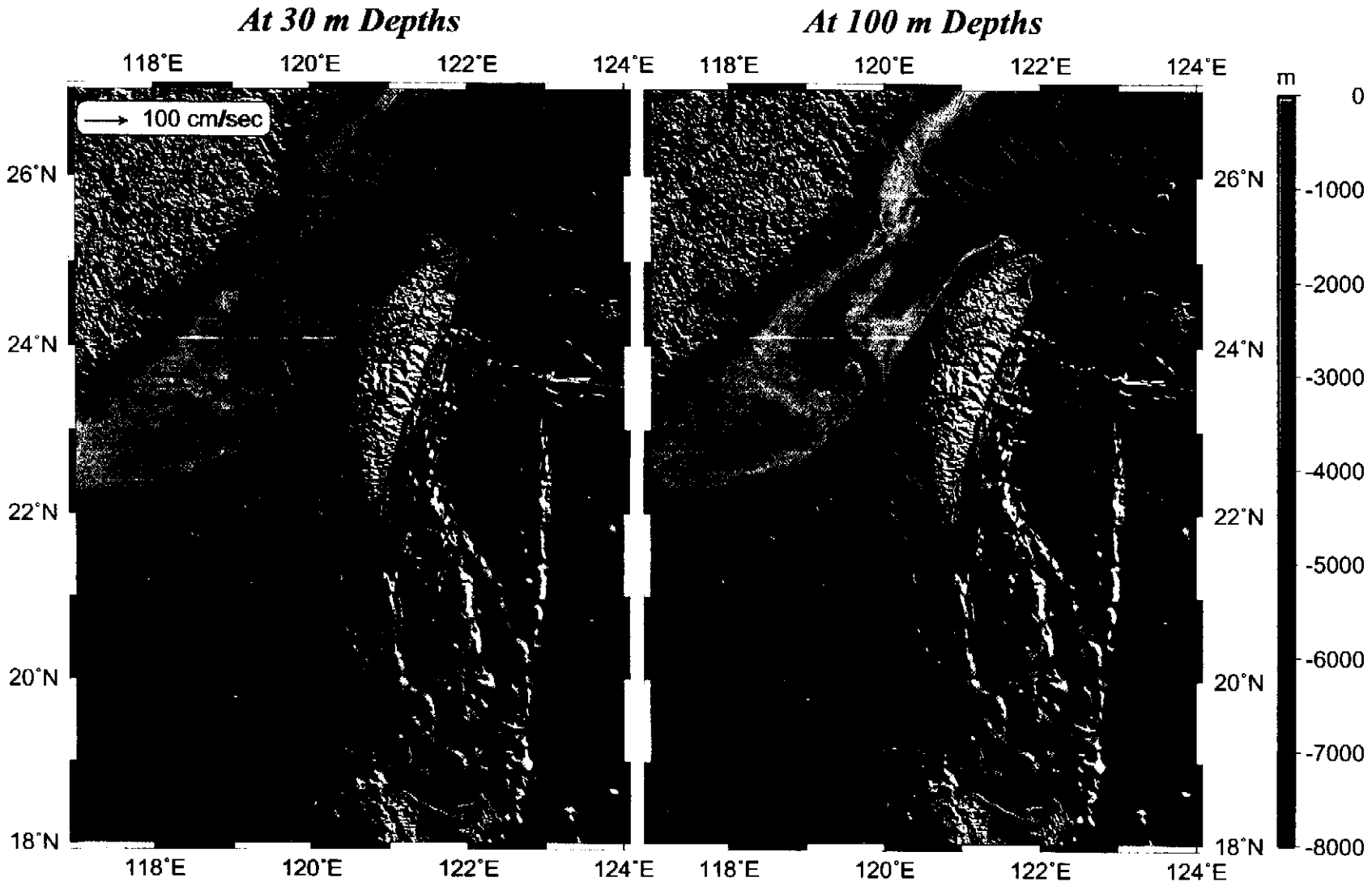
At 30 m Depths
At 100 m Depths
118°E
120°E
122°E
124°E
26°N
24°N
22°N
20°N
18°N
100 cm/sec
m
0
-1000
-2000
-3000
-4000
-5000
-6000
-7000
-8000

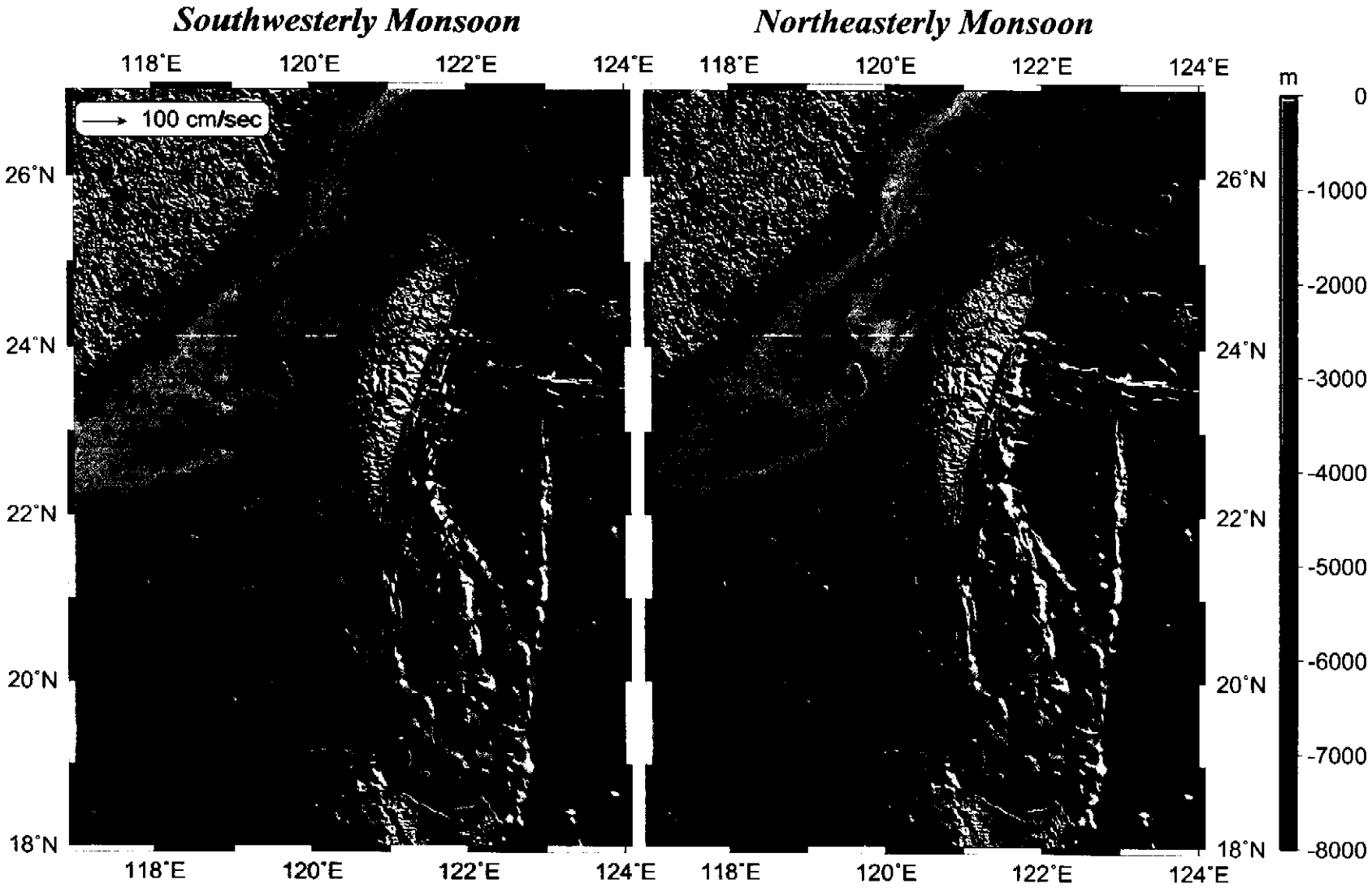
Southwesterly Monsoon
Northeasterly Monsoon
100 cm/sec
118°E
120°E
122°E
124°E
26°N
24°N
22°N
20°N
18°N
m
0
-1000
-2000
-3000
-4000
-5000
-6000
-7000
-8000

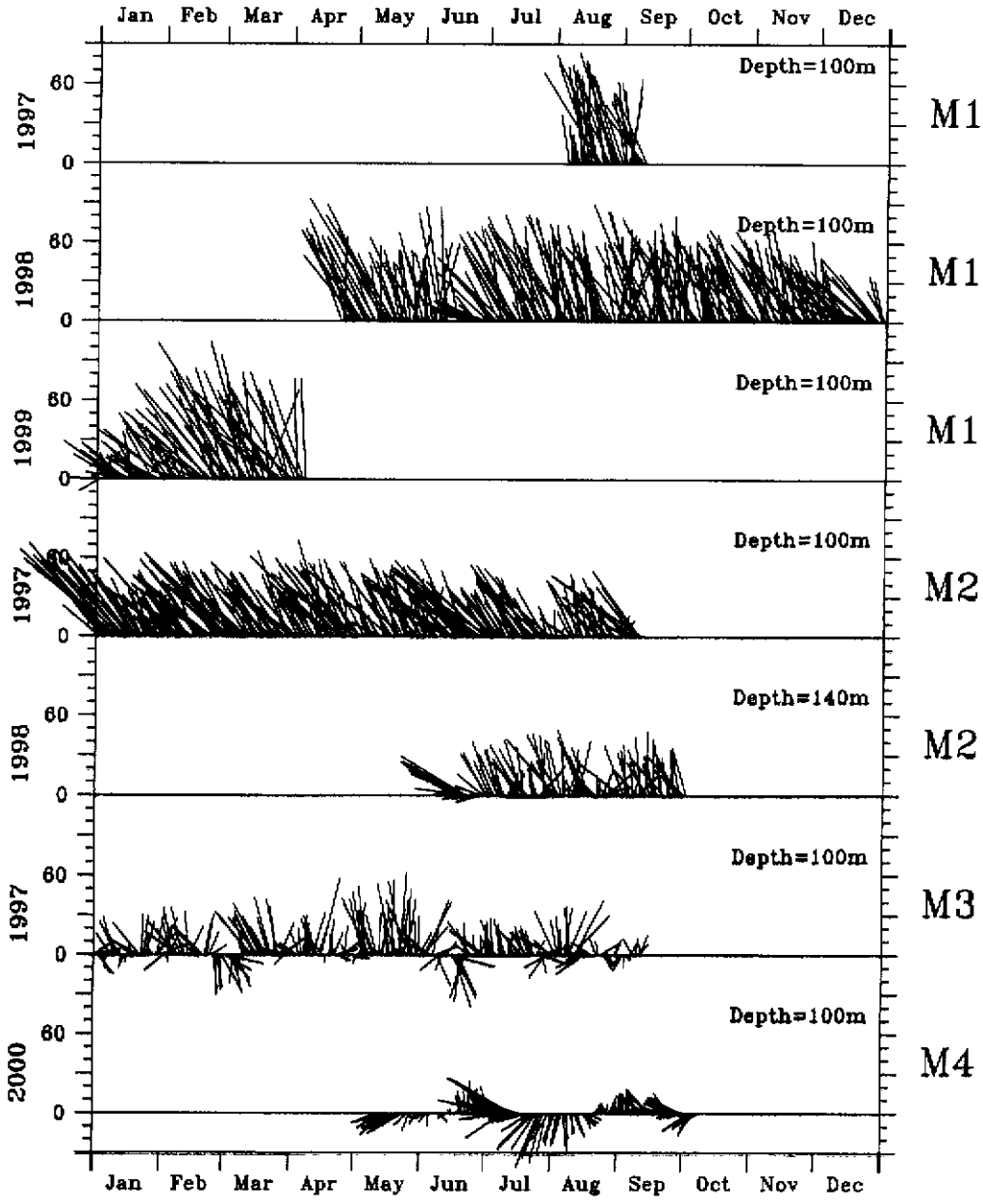
Jan Feb Mar Apr May Jun Jul Aug Sep Oct Nov Dec
1997
Depth=100m
M1
1998
Depth=100m
M1
1999
Depth=100m
M1
1997
Depth=100m
M2
1998
Depth=140m
M2
1997
Depth=100m
M3
2000
Depth=100m
M4
60
0
Jan Feb Mar Apr May Jun Jul Aug Sep Oct Nov Dec

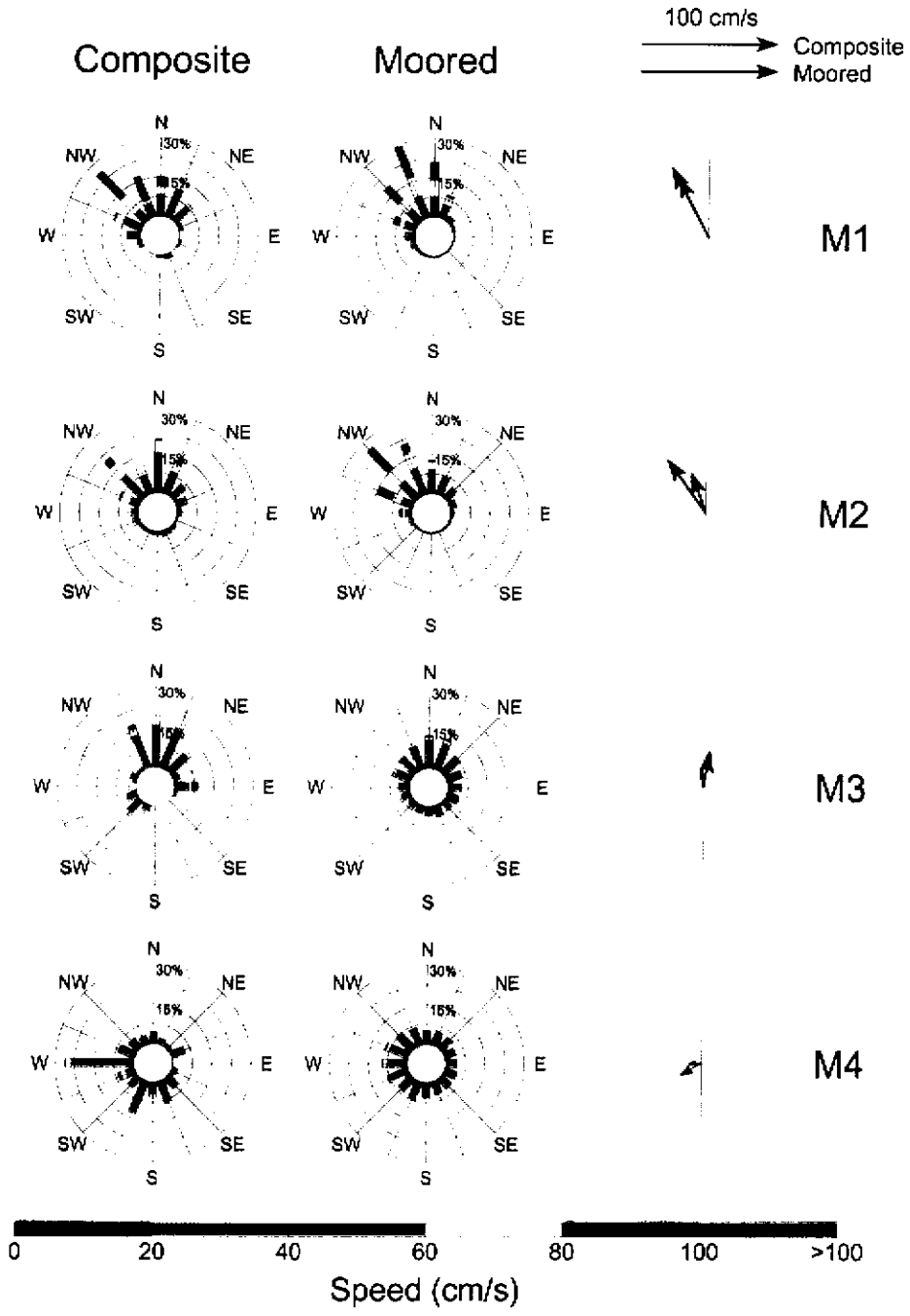
Composite
Moored
100 cm/s
Composite
Moored
N
NE
E
SE
S
SW
W
NW
30%
15%
M1
M2
M3
M4
0
20
40
60
80
100
>100
Speed (cm/s)

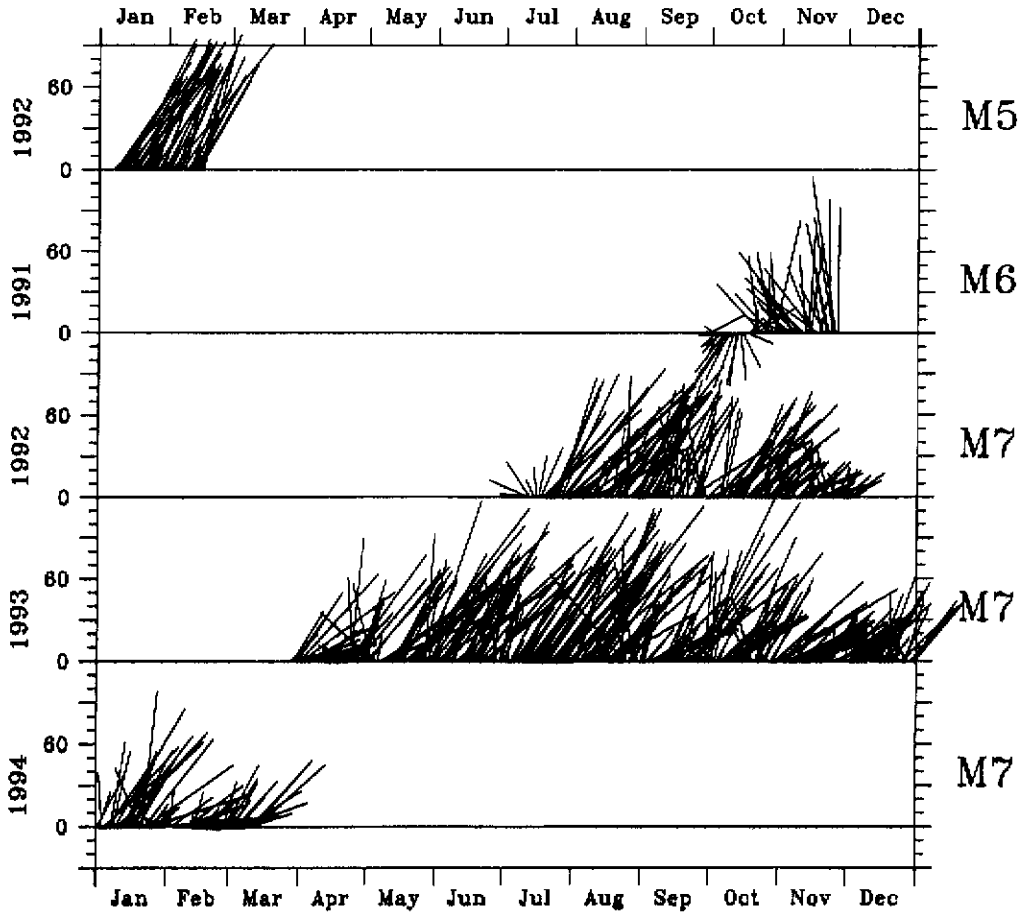
Jan
Feb
Mar
Apr
May
Jun
Jul
Aug
Sep
Oct
Nov
Dec
1992
1991
1992
1993
1994
60
0
M5
M6
M7
M7
M7

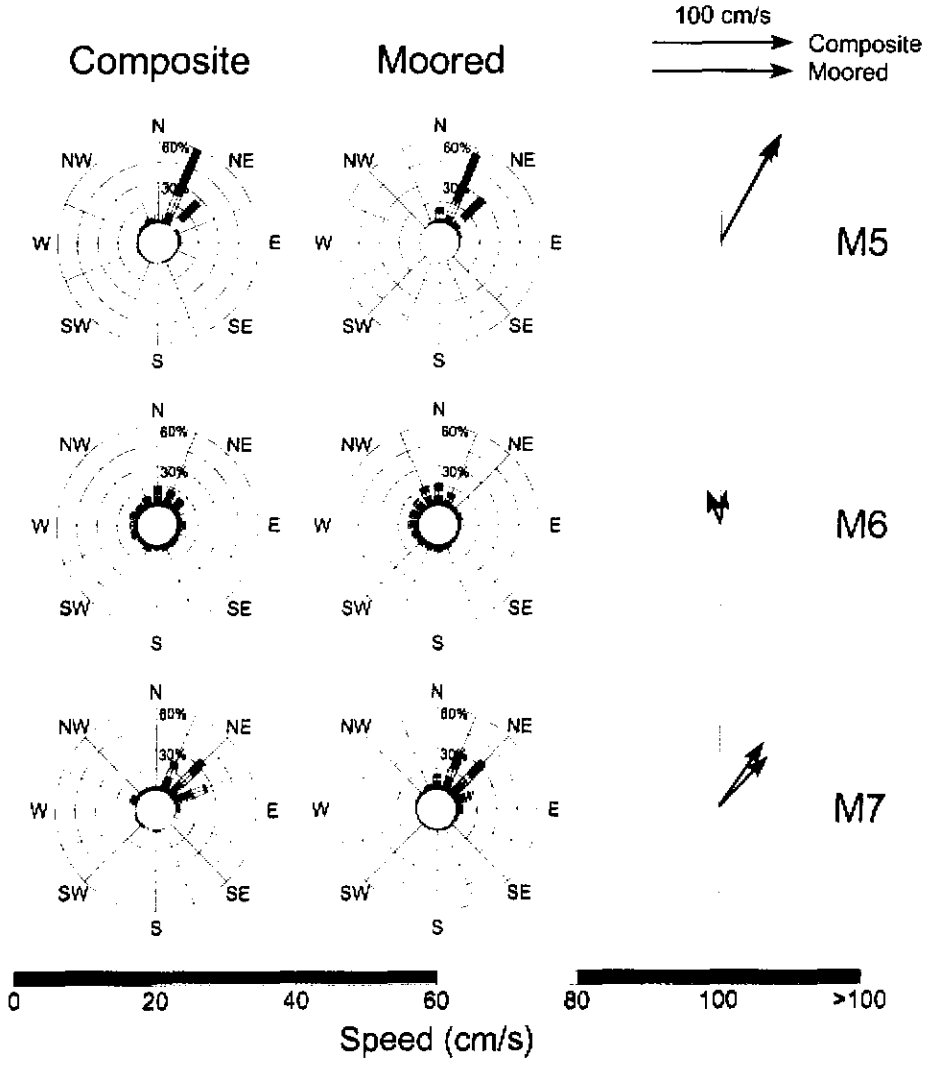
Composite
Moored
100 cm/s
Composite
Moored
N
NE
E
SE
S
SW
W
NW
60%
30%
M5
M6
M7
0
20
40
60
80
100
>100
Speed (cm/s)

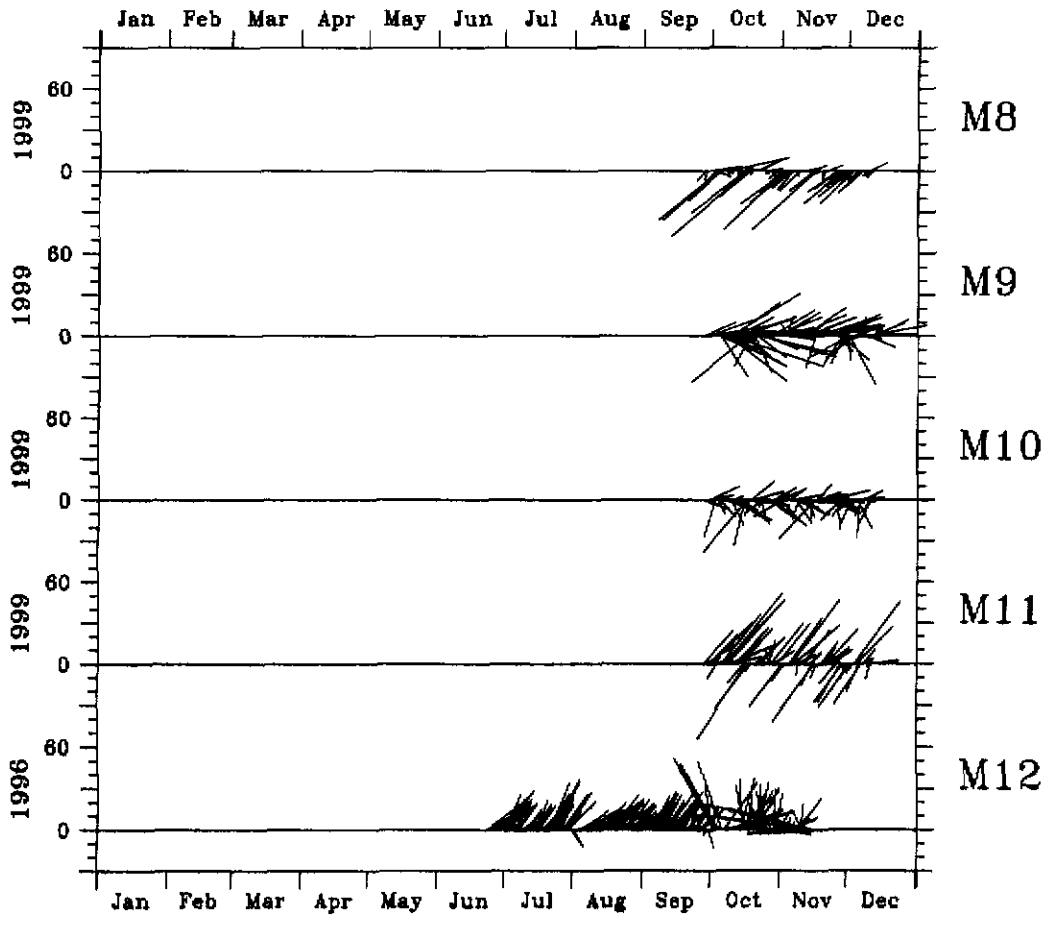
Jan
Feb
Mar
Apr
May
Jun
Jul
Aug
Sep
Oct
Nov
Dec
60
0
1999
M8
M9
M10
M11
M12
1996

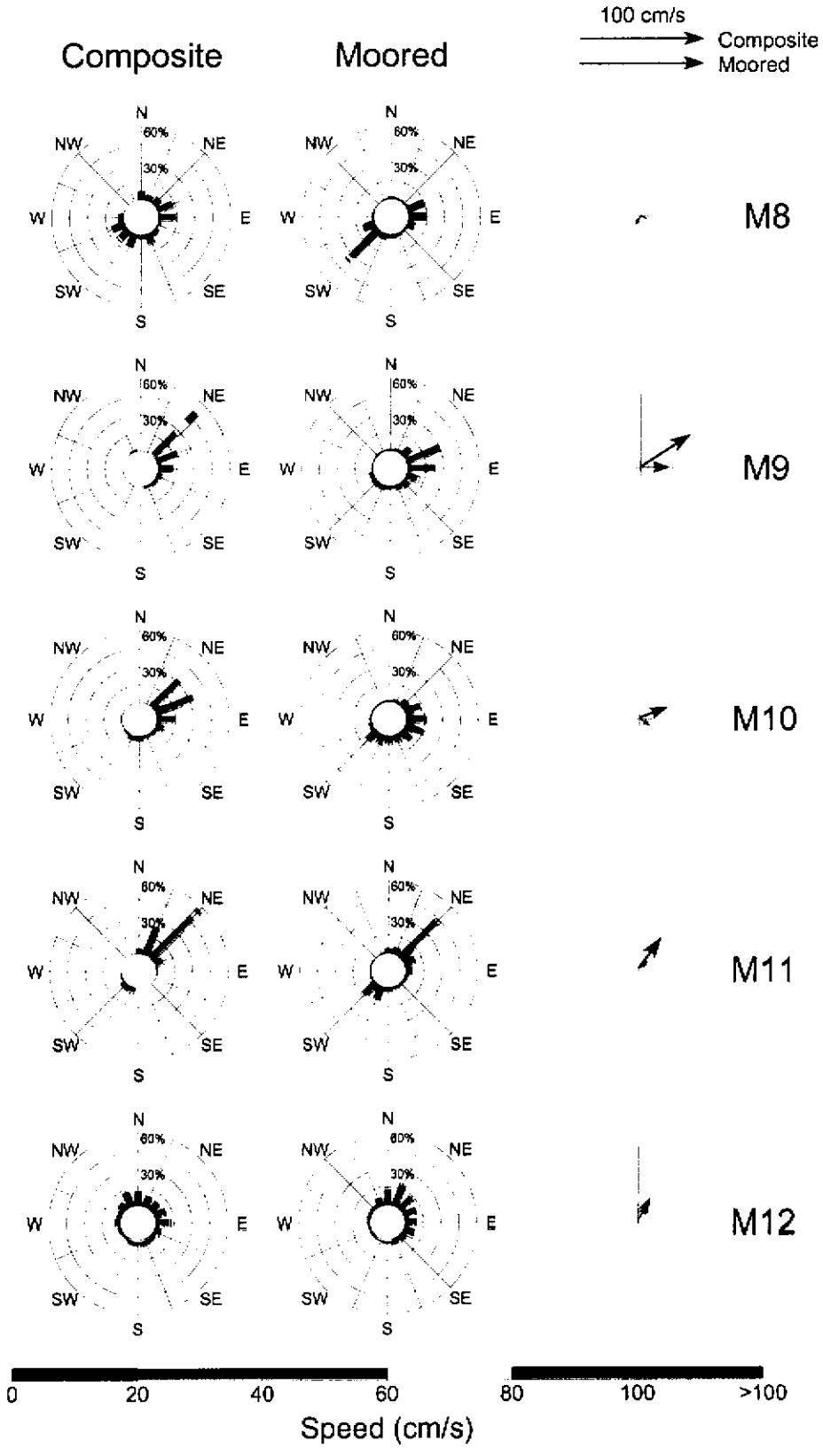
Composite
Moored
100 cm/s
Composite
Moored
N
NE
E
SE
S
SW
W
NW
60%
30%
M8
M9
M10
M11
M12
0
20
40
60
80
100
>100
Speed (cm/s)

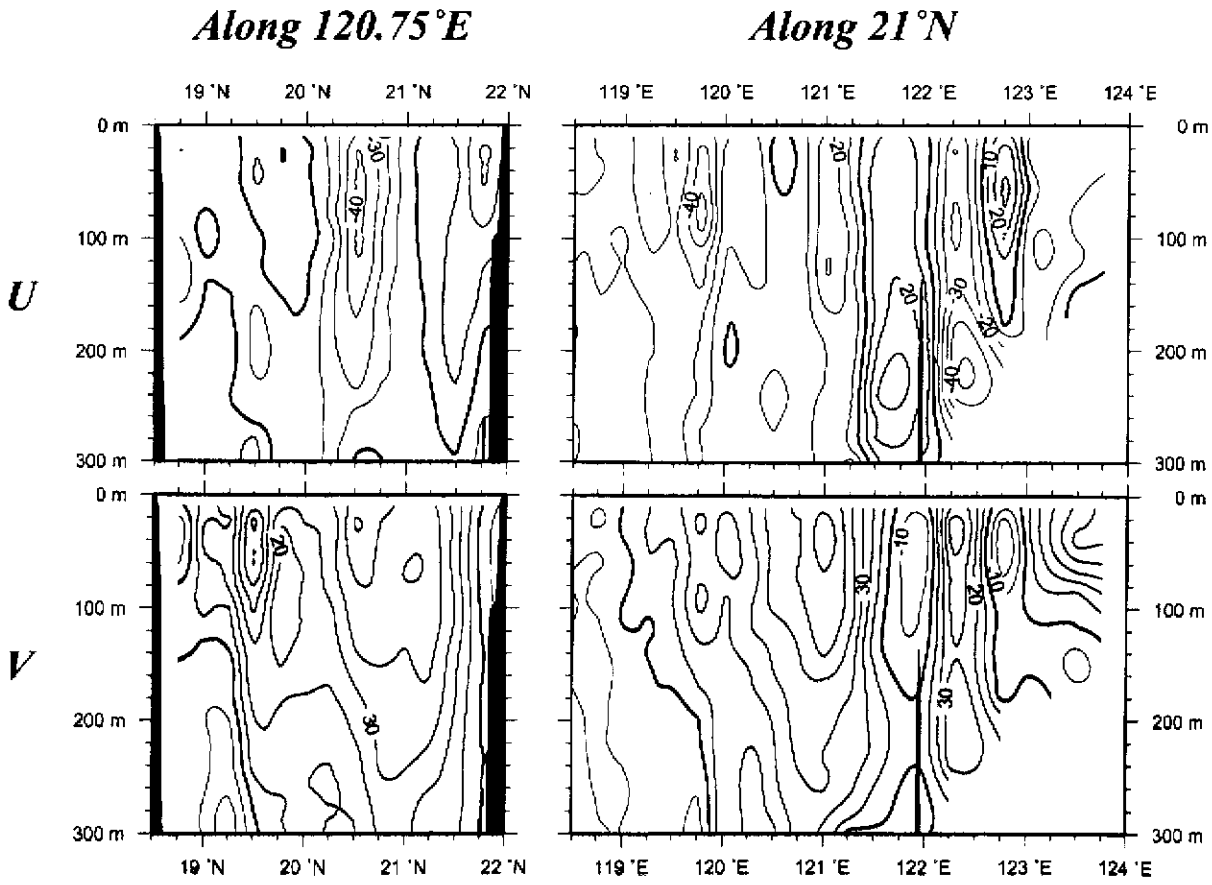
Along 120.75°E
Along 21°N
U
V
19 °N
20 °N
21 °N
22 °N
119 °E
120 °E
121 °E
122 °E
123 °E
124 °E
0 m
100 m
200 m
300 m

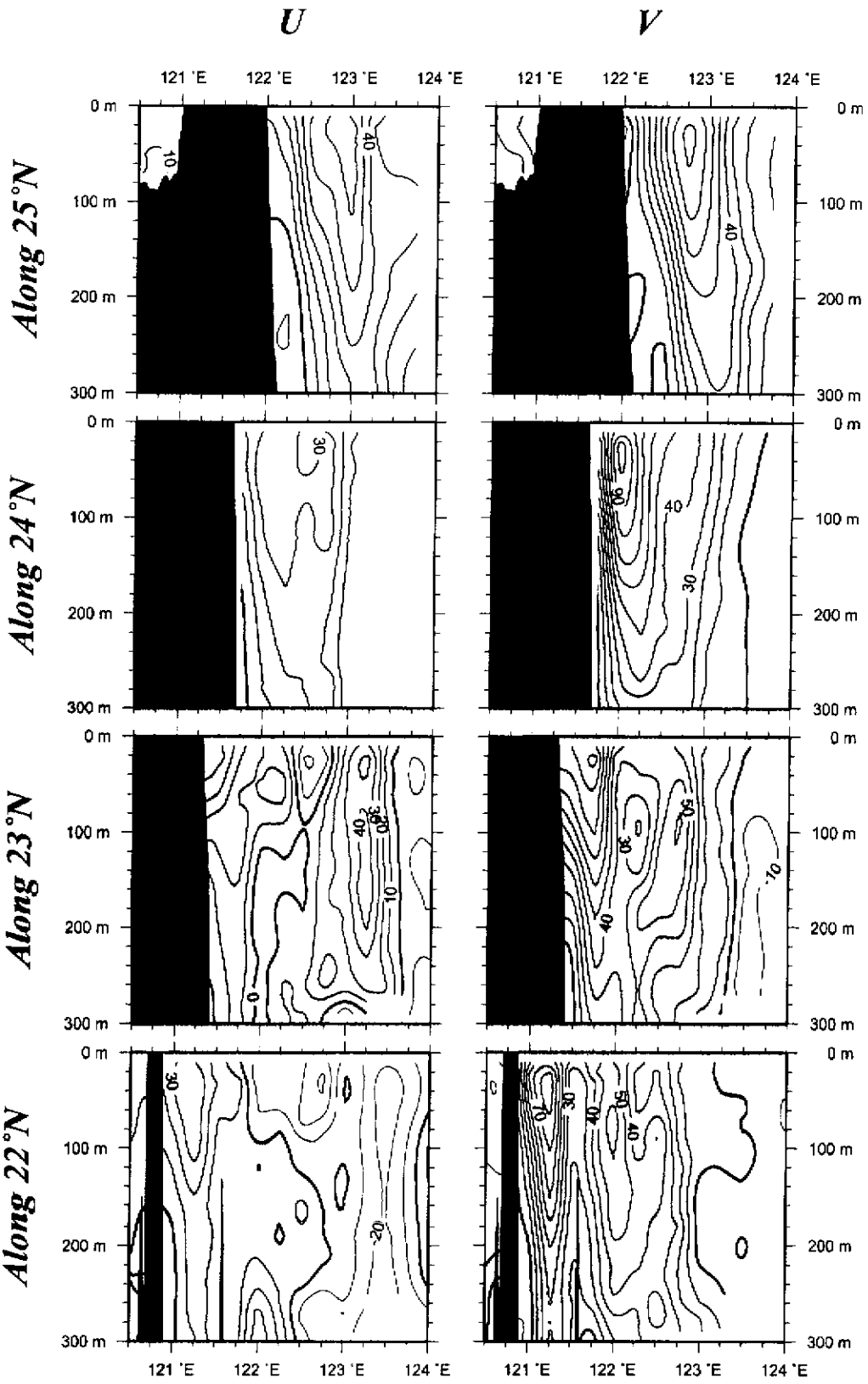
U
V
Along 25°N
Along 24°N
Along 23°N
Along 22°N
121 °E
122 °E
123 °E
124 °E
0 m
100 m
200 m
300 m

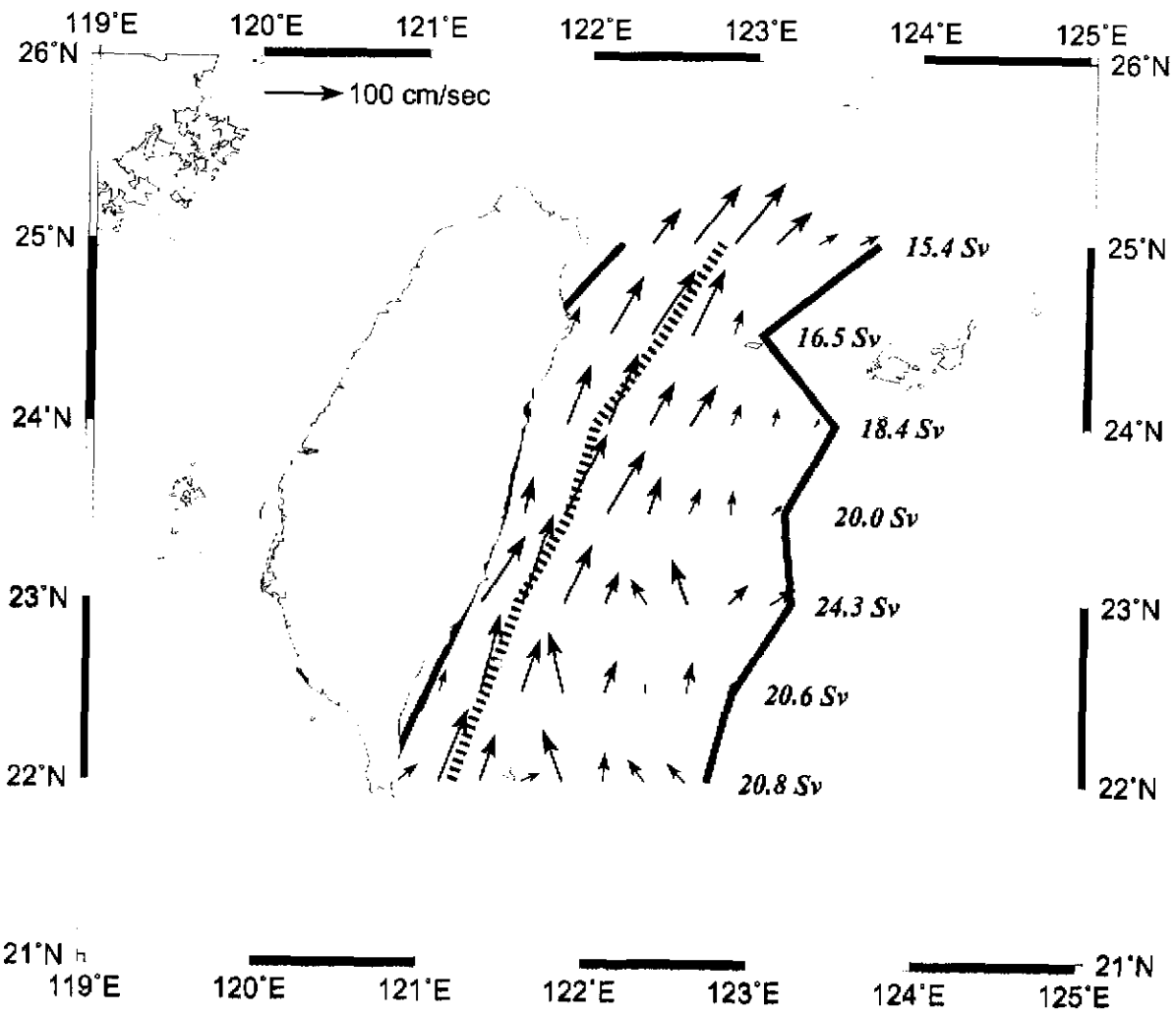
119°E
120°E
121°E
122°E
123°E
124°E
125°E
26°N
25°N
24°N
23°N
22°N
21°N
100 cm/sec
15.4 Sv
16.5 Sv
18.4 Sv
20.0 Sv
24.3 Sv
20.6 Sv
20.8 Sv

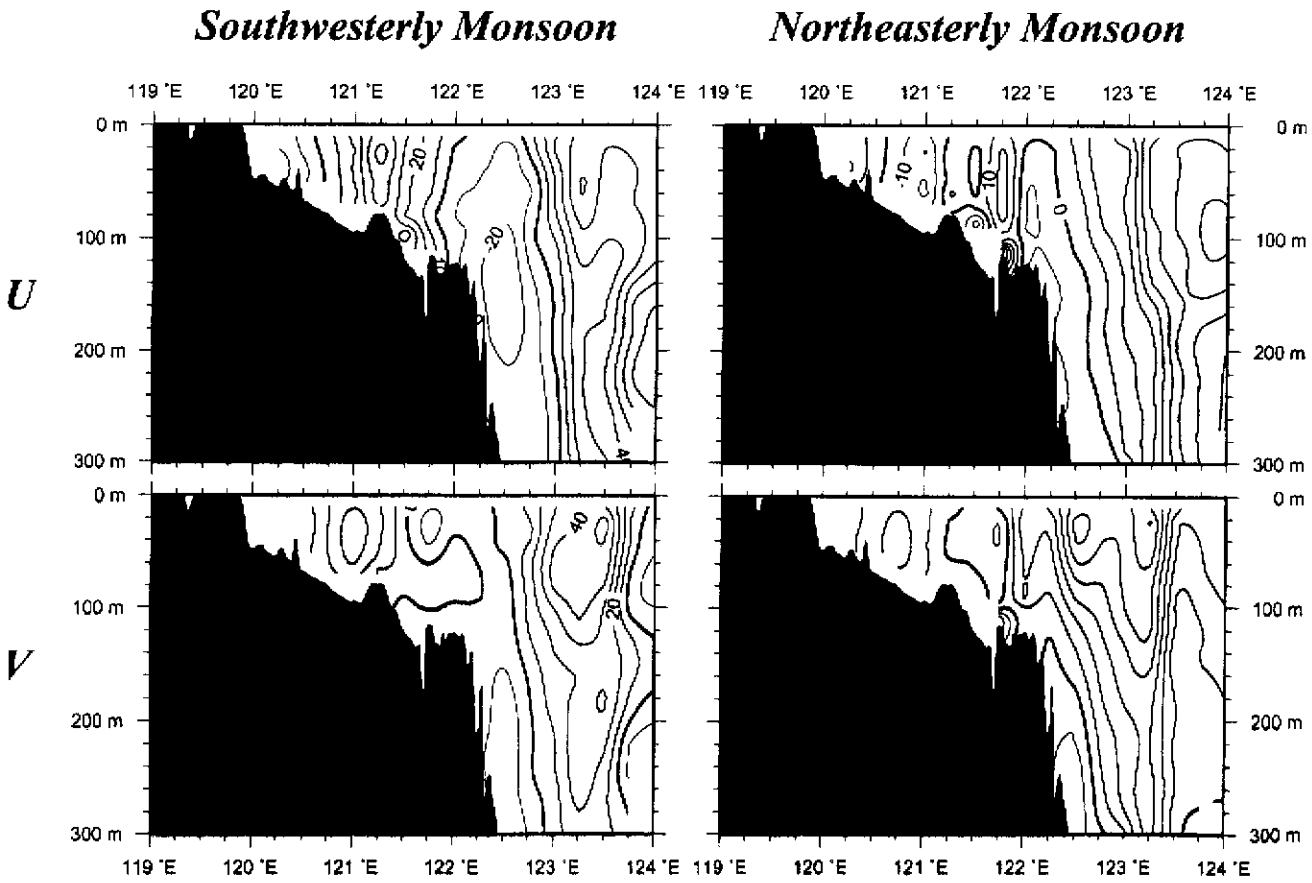
Southwesterly Monsoon
Northeasterly Monsoon
U
V
119 °E
120 °E
121 °E
122 °E
123 °E
124 °E
0 m
100 m
200 m
300 m

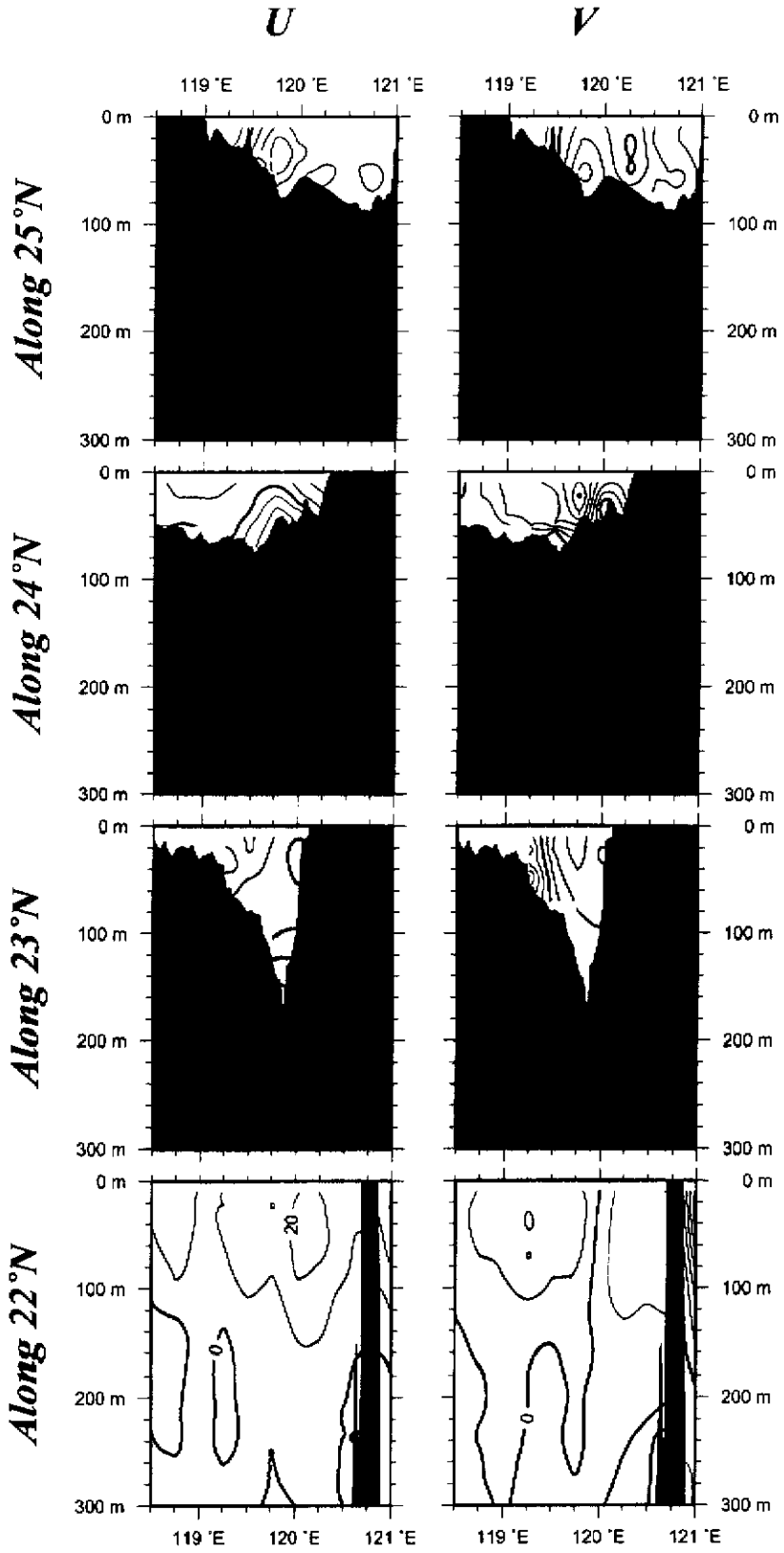
U
V
119 °E
120 °E
121 °E
0 m
100 m
200 m
300 m
Along 25°N
Along 24°N
Along 23°N
Along 22°N
20
0
0
0